

# MECH 451/452

## PROJECT REPORT

---

Praxim

### Three-Dimensional Haptic Emulation of Hard Surfaces with Applications to Orthopaedic Surgery

Authors:

Sean Fabris (69499044)

Arya Oskui (64201049)

Anthony Pak (82230046)

Brad Roger (36049054)

Sina Sajadian (63155048)

Adnan Siddiqui (67390047)

Submitted to:

Dr. Xiaodong Lu

Assistant Professor

Department of Mechanical Engineering

University of British Columbia

Submitted on:

May 1st, 2009

## **Abstract**

Total Knee Arthroplasty (TKA) is an orthopaedic surgery in which an implant is inserted into a damaged knee to improve its function. Modern practice attempts to minimize tissue removal and damage during surgery, so bone-conserving implants that replicate the natural bone structure of the knee are used to reduce the amount of bone and tissue removed during TKA. Curvilinear cuts must be made by a surgeon in order to install the implants. Currently, there is no commercial technology that can model such complex curvilinear surfaces accurately and reliably enough to guide a surgeon during surgery. As such, the objective of this project was to develop a proof-of-concept prototype of a small, semi-active, bone-mounted cutting guide with applications to TKA. An existing haptic hard surface emulation technique was studied extensively and improved upon for the developed prototype to model three-dimensional curvilinear surfaces.

The design objectives for the prototype were for it to be able to emulate a realistic stiff surface, model surface rigidity accurately, allow smooth surface tracing for predefined surface patterns, provide unimpeded motion away from surface constraints, and be intuitive and safe to use. A holistic mechatronics approach was used to meet the objectives and functional requirements determined for the prototype. In particular, the design was divided into four main categories – mechanical, electrical, controls system and algorithm – and detailed concepts were developed and evaluated for each category. A fully functional prototype that integrated the four categories was manufactured and tested to validate that it met the functional requirements.

Tests of the prototype's ability to emulate rigid, virtual surfaces in two- and three-dimensions proved were very successful. The prototype received positive qualitative feedback from users and yielded quantitative results that met the project requirements. The design is a significant improvement over the previous haptic emulation technology and suggests that, with further development, haptic emulation technology has the potential to be commercially viable for applications involving orthopaedic surgery. The qualitative and quantitative test results were used in conjunction with identified behavioural characteristics and design issues to provide recommendations for future work.

## Table of Contents

Abstract.....	ii
List of Figures .....	v
List of Tables .....	viii
1. Introduction.....	1
2. Project Background.....	3
2.1 Introduction to Hard Surface Emulation .....	3
2.2 Existing Commercial Technologies .....	6
2.2.1 Acrobot Concept .....	7
2.2.2 Cobot Concept .....	8
2.2.3 PADyC Concept .....	9
2.2.4 PTER Dissipative Passive Concept .....	10
2.2.5 Mako Haptic Guidance System Concept.....	11
2.3 Previous Technology Developed for Praxim .....	12
2.3.1 Description of Hungr’s Prototype .....	13
2.3.2 Identified Problems.....	15
3. Functional Requirements .....	17
3.1 Project Scope.....	17
3.2 Design Objectives .....	18
3.3 Evaluation Criteria .....	19
4. Concept Generation and Evaluation .....	21
4.1 Initial Concept Evaluation.....	21
4.2 Detailed Concept Evaluation.....	28
4.2.1 Rotational Joints Concepts.....	28
4.2.2 Linear Bearing Concepts .....	35
4.2.3 Controls Architecture .....	36
5. Design and Analysis .....	38

5.1	Mechanical Design.....	38
5.1.1	Purchased Components .....	39
5.1.2	Manufactured Components.....	43
5.2	Electrical Design .....	51
5.2.1	Encoders.....	51
5.2.2	Motor and Motor Controller.....	54
5.2.3	Microcontroller .....	55
5.3	Control System Design.....	56
5.3.1	Control System Architecture.....	56
5.3.2	User Interface.....	57
5.3.3	Controller Design .....	60
5.4	Algorithm Design.....	64
6.	Testing and Results .....	67
6.1	X-Y Plane 2-D Test Results .....	67
6.2	Y-Z Plane 2-D Test Results .....	70
6.3	3-D Milling Tests .....	71
7.	Future Work.....	76
7.1	Future Mechanical Work.....	76
7.2	Future Electrical and Controls Work .....	82
8.	Conclusion .....	84
9.	References.....	85
	Appendix A – Assembly and Engineering Drawings .....	A
	Appendix B – Data Sheets for Major Components .....	B
	Appendix C – Budget.....	C

## List of Figures

Figure 1 - Acrobot Sculptor (photo courtesy of Acrobot Precision Surgical Systems).....	7
Figure 2 - Three region stiffness model (Harris, Davies and Jakopec 2004) .....	8
Figure 3 - Cobot concept (Peshkin et al., 1996) .....	9
Figure 4 - PADyC freewheel concept (Troccaz 1996) .....	10
Figure 5 - PTER dissipative passive device (Book et al., 1996).....	11
Figure 6 - Mako haptic guidance system (photo courtesy of Mako Surgical Corp.).....	12
Figure 7 - Original Praxiteles model (photo courtesy of Christopher Plaskos).....	13
Figure 8 - Hungr's haptic feedback prototype (2008) .....	14
Figure 9 - Block diagram of Hungr's prototype (2008) .....	14
Figure 10 - Distal femur (left); simplified model (right) .....	22
Figure 11 - Sample K'NEX prototype.....	23
Figure 12 - Angle of attack .....	24
Figure 13 - Rotational base with two linear sliders .....	25
Figure 14 - Two rotational joints with a linear slider .....	25
Figure 15 - Ball joint with a linear slider.....	26
Figure 16 - More detailed rotational base with two linear sliders .....	26
Figure 17 - More detailed two rotational joints with a linear slider .....	27
Figure 18 - More detailed ball joint with a linear slider .....	27
Figure 19 - Sheet metal design.....	28
Figure 20 - Exploded view of sheet metal design.....	29
Figure 21 - Thrust bearing design.....	30
Figure 22 - Three-dimensional cutaway of thrust bearing design .....	31
Figure 23 - Bearing design considerations.....	31
Figure 24 - Exploded view of thrust bearing design.....	32
Figure 25 - Exploded view of critical parts at joint 2 .....	32
Figure 26 - Angular contact bearings concept .....	33
Figure 27 - Design 1 for the linear bearing.....	35
Figure 28 - Design 2 for the linear bearing.....	36
Figure 29 - Final design with axis, link and encoder numbers .....	38
Figure 30 - Angular contact bearings orientation .....	39

Figure 31 - Back-to-back bearing orientation.....	40
Figure 32 - Force pathway .....	40
Figure 33 - Linear ball bearing .....	41
Figure 34 - Linear ball bearing finite element analysis .....	42
Figure 35 - Bone mount .....	43
Figure 36 - Link 1 .....	44
Figure 37 - Link 1 finite element analysis .....	44
Figure 38 - Link 2 .....	46
Figure 39 - Link 2 finite element analysis .....	47
Figure 40 - Link 3 .....	47
Figure 41 - Motor and Encoder 1 support.....	48
Figure 42 - Encoder 2 support .....	49
Figure 43 - Motor stopper .....	49
Figure 44 - Linear encoder support.....	50
Figure 45 - Slider mounting plate .....	50
Figure 46 - Axis 1 rotary encoder (left); Axis 2 rotary encoder (right).....	52
Figure 47 - Maxon EC-Max motor .....	54
Figure 48 - Development board for Atmel AT90CAN128.....	55
Figure 49 - Control system architecture.....	56
Figure 50 - User interface and control board .....	58
Figure 51 - "Home" position.....	59
Figure 52 - EPOS 24/5 block diagram (photo courtesy of Maxon Motor Control).....	60
Figure 53 - Magnitude vs. frequency for load test.....	61
Figure 54 - Phase vs. frequency for load test.....	61
Figure 55 - Step response ( $K_P = 64$ , $K_I = 0$ , $K_D = 20$ ) .....	62
Figure 56 - Step response ( $K_P = 64$ , $K_I = 0$ , $K_D = 50$ ) .....	63
Figure 57 - Step response ( $K_P = 100$ , $K_I = 10$ , $K_D = 200$ ) .....	63
Figure 58 - Hungr's linkage orientation .....	64
Figure 59 - Blocker position algorithm.....	65
Figure 60 - Accessible regions of prototype .....	67
Figure 61 - X-Y plane setup.....	68

Figure 62 - X-Y plane 2-D test: straight line .....	68
Figure 63 - X-Y plane 2-D test: ellipse.....	69
Figure 64 - X-Y plane 2-D test: sine bump.....	70
Figure 65 - Y-Z plane test setup .....	70
Figure 66 - Y-Z plane 2-D test: sine bump .....	71
Figure 67 - Y-Z plane 2-D test: ellipse .....	71
Figure 68 - 3-D free space test setup .....	72
Figure 69 - 3-D test profiles: flat plane.....	73
Figure 70 - 3-D test profiles: sine bump .....	73
Figure 71 - 3-D test profiles: ellipsoid.....	74
Figure 72 - 3-D milling test setup .....	74
Figure 74 - General purpose, open ball bearing.....	77
Figure 75 - Linear ball bearing with sliding rail .....	77
Figure 75 - Linear encoder with stand .....	78
Figure 76 - Link 3 .....	78
Figure 77 - Motor and motor blocker .....	79
Figure 78 - Motor stopper and screw .....	79
Figure 79 - Section view of the shoulder screws used for Axis 1 and 2.....	80
Figure 80 - Spherical milling bit.....	80
Figure 81 - Encoder connections with flexible couplings .....	81

## **List of Tables**

Table 1 - Maximum stiffness of commercially available haptic devices (Hungar 2008).....	5
Table 2 – Functional requirements and evaluation criteria.....	19
Table 3 - Permutations for three-dimensional motion with three links .....	22
Table 4 - Evaluation of permutations.....	23
Table 5 - Rotary encoder selection process .....	51
Table 6 - Linear encoder alternatives.....	53
Table 7 - Encoder resolution analysis.....	54
Table 8 - Fixed controller parameters.....	60



## 1. Introduction

This project was a continuation of the work completed in two previous thesis projects by Dr. Christopher Plaskos and Nikolai Hungr at l'Université Joseph Fourier in Grenoble, France and at the University of British Columbia, Vancouver, Canada, respectively. The clients for the project were Dr. Plaskos of Praxim, and his liaison at the University of British Columbia, Dr. Antony Hodgson, Associate Professor in the Mechanical Engineering Department. The purpose of the previous two projects was to improve femoral implant positioning and fit in total knee arthroplasty (TKA) by developing semi-active, bone-mounted cutting guides.

Knee arthroplasty is an orthopaedic surgery in which a damaged or dysfunctional joint surface in the knee is replaced with an implant to improve its function. The purpose of developing robotic technology to assist in surgery is to reduce surgery time while maintaining patient safety and allowing the surgeon to retain ultimate control over the surgery. The first robot developed by Plaskos, Praxiteles, allowed surgeons to mill in the five respective planes of a conventional distal femoral implant, which increased precision and control during surgery. Hungr's project was a continuation of this, the objective of which was to expand Praxiteles' capabilities to include curvilinear bone sculpting. A curvilinear sculpting technique was developed to facilitate the use of "bone-conserving" implants. Bone conserving implants are designed to mate with bone surfaces and approximate the natural curvature of bone structures, which minimizes the amount of bone and tissue that has to be removed during surgery (thereby reducing the damage caused by the surgery). Hungr developed a physical prototype which demonstrated a novel haptic method for emulating a hard, two-dimensional curvilinear surface using a pen – in place of a surgical tool – as the end-effector. Although Hungr's prototype successfully demonstrated his concept, he identified several behavioural issues and limitations with his prototype (Hungr 2008). The objective of this project was to expand on the work done by Plaskos and Hungr to develop a prototype that applies haptic hard surface emulation techniques to three-dimensional curvilinear surfaces and resolves the behavioural issues and limitations of the previous projects.

Although both previous projects focused on knee arthroplasties, the rationale for continuing to develop the technology is to be able to apply it to other surgeries in the future (e.g. hip

replacement). That being said, such a product will only be marketable if it can simultaneously speed up existing surgeries, help surgeons perform the surgeries better, *and* reduce the overall cost of the surgeries. As such, it is imperative that any future versions of the technology not only improve on surgery quality, but also keep product costs low and be able to reduce surgery times enough to justify the tool's cost. Given that no current technology completely meets the requirements for total knee arthroplasty using haptic control techniques, and that a technology that could meet those requirements would be beneficial for surgeons and patients alike, continuing with Hungr's and Plaskos' work was a logical step.

This report describes the design process used to develop a physical prototype that satisfies the project requirements. It provides some background information about the project, outlines the functional requirements, reviews the concept generation process and the criteria used to evaluate the concepts, describes the final design of the prototype, examines test results, discusses potential future work, and provides conclusions about the design process.

## **2. Project Background**

Significant research has been performed to develop technology that minimizes tissue removal during orthopaedic surgery to satisfy the surgical community's desire for tissue conservation. One such area of research is the development of hard surface emulation techniques to restrict a surgeon's motion to a virtual three-dimensional region. These types of systems are useful for orthopaedic surgery because they can be used to prevent cutting tools from damaging soft tissue located next to the surgical area. Hungr's work focused on developing a novel haptic method of emulating a hard, curvilinear surface for use during knee arthroplasty. In addition, previous technologies have attempted to implement haptic techniques for knee surgery. Both have been relatively successful with respect to speed and accuracy, but have not provided completely realistic hard surface emulations and have had many limitations. As such, the objective of this project was to improve upon existing haptic methods to emulate a hard, curvilinear surface in three-dimensions. This section briefly introduces the concept of hard surface emulation, discusses some commercial technologies that Hungr researched that implement user control and hard surface constraints, and then discusses the work done by Plaskos and Hungr for Praxim.

### **2.1 Introduction to Hard Surface Emulation**

Hard surface emulation can be defined as "the ability of a manipulator to simulate a rigid virtual surface of relatively arbitrary shape" (Hungr 2008). In other words, hard surface emulation – also known as haptic force feedback – allows a manipulator to move freely in space until it reaches a predefined position or surface, at which point the manipulator experiences a virtual "hard" force that inhibits its movement past the position or surface. In computer-assisted surgical procedures (such as the one this project was developed for), hard surface emulation is primarily used to restrict a surgeon from placing a cutting tool into a dangerous or sensitive region. Several studies have been performed to demonstrate the importance of hard surface emulation in orthopaedic surgery and to further the development of haptic interface design for applications involving the bone removal (Ho et al., 1995; Shoham et al., 2003; Brisson et al., 2004; Roche, 2006). Although these studies have been limited in scope and are only preliminary in nature, they have yielded important design constraints. An effective surgical haptic force feedback system must not only





restrict movement but also must not interfere with the surgery itself either by physically impeding surgery or by creating instability in the cutting tool. A hard surface emulator must allow the surgeon to complete a surgery efficiently and accurately while defining the restricted surface with enough precision and stiffness such that he feels that the virtual surface he is interacting with is a real surface. Salisbury et al. summarized the objectives that should be satisfied when design a haptic force feedback system (1995):

- When not in contact with the surface, the user has complete freedom of motion;
- The stiffness of the surface is, for all practical purposes, infinitely high regardless of the speed or direction of the user's motion; and,
- The surface can be traced smoothly and exactly.

Hard surface emulation can be achieved using a variety of methods that use both electrical and physical principles. Most previous research has focused on using electrical techniques to implement hard surface emulation, whereas Hungr's research used a mechatronics approach to implement haptic feedback. The electrical techniques have typically used algorithms that use changes in impedance to control motor torque and restrict the movement of a manipulator based on its position determined by a number of sensors (Hayward and MacLean 2007). The algorithms generally use sensors to determine when a manipulator breaches a virtual surface, at which point motor torque is changed to limit or stop the motion of the manipulator. The effectiveness of these methods is limited by the fact that a slight penetration of the virtual surface is required: hardware and software limitations such as response lag time, joint backlash, structural flex, and sensor noise make it extremely difficult to measure such penetration with accuracy and precision (Hungr 2008). This makes it difficult to emulate a hard surface without generating instability in the system because the system typically bounces at the virtual surface (Salisbury et al., 1995; Hayward & MacLean, 2007). Hungr's research used an integrated mechatronics system with modified control algorithms and mechanical concepts to resolve many, but not all, of the problems with the electrical methods. His work is discussed further in Section 2.3.

Lawrence and Chapel (1994) state that a stiffness of at least  $10 \text{ kNm}^{-1}$  is required for a human being to perceive a surface as being “hard”. As discussed in Section 3,  $10 \text{ kNm}^{-1}$  was used during design as the minimum acceptable stiffness for a haptic force feedback prototype to be considered adequate. For reference purposes, Kuchenbecker et al. (2006) and Hayward and MacLean (2007) report that true metal-metal contact stiffness is around  $1000 \text{ kNm}^{-1}$ . Table 1 lists the maximum stiffness values for several common haptic feedback devices (Hung 2008).

**Table 1 - Maximum stiffness of commercially available haptic devices (Hung 2008)**

Haptic device	Photo of device	Maximum stiffness ( $\text{kNm}^{-1}$ )
Haption Virtuose		2
MPB Freedom		2
Sensable Phantom		2
Mimic Mantis		5.5

Force Dimension Omega		14.5
Moog FSC Robotics HapticMASTER		50

It can be seen that the majority of the devices do not meet the  $10 \text{ kNm}^{-1}$  stiffness requirement determined by Lawrence & Chapel. Moreover, the devices presented are only haptic feedback devices and not necessarily hard surface emulators. As such, they do not satisfy the requirements for a surgical cutting tool with haptic force feedback because they do not combine the properties of haptic feedback with hard surface emulation. Section 2.2 discusses previous technology that uses haptic feedback to emulate hard surfaces.

## 2.2 Existing Commercial Technologies

Significant research has been performed in the field of hard surface emulation. Several commercial products have been developed for guided motion control applications similar to guided surgery. Several concepts are discussed in this report: Acrobot, Cobot, PADyC, and PTER. Important features, advantages and disadvantages of each system are discussed; these are then used to formulate the requirements for a three-dimensional hard surface emulation device with applications to orthopaedic surgery in Section 3.

### 2.2.1 Acrobot Concept

One of the most successful commercial technologies to date is the Acrobot (Active Constraint Concept), shown in Figure 1, developed by Harris et al. (2004).



**Figure 1 - Acrobot Sculptor (photo courtesy of Acrobot Precision Surgical Systems)**

The Acrobot is primarily used for three-dimensional cutting tool guidance during knee arthroplasties. It uses sensors to detect a user's input force and counteracts that force near the boundary surface by varying impedance and translating it into "stiffness", and adjusts the robot to reach a desired position based on the current position. The algorithm for the system adjusts the impedance by adjusting the proportional and derivative gains of the system's controller. The device uses three "regions" to incrementally increase stiffness. Figure 2 illustrates the model: Region 1 is where the user can move without restriction, Region 2 is where the stiffness of the robot increases to warn the user he is approaching a restricted area, and Region 3 is where the user can not penetrate. Region 2 is essentially a small zone around the boundary where the stiffness felt by the user increases from a negligible amount to the amount required for a user to feel that there is a hard surface. This serves as a "transition" zone between free and restricted motion in order to minimize instability at the virtual hard surface and to mitigate the risk of penetrating the surface due to delays in the control system. These properties, however, mean that the zone has a springy feel and restricts motion along the boundary because of the increased

impedance (Hung 2008). The effect of impedance is particularly important because it is a property inherent with electrical haptic systems and is a primary reason to use a mechatronics system. There is also a relatively high amount of friction that restricts free motion away from the restricted boundary.

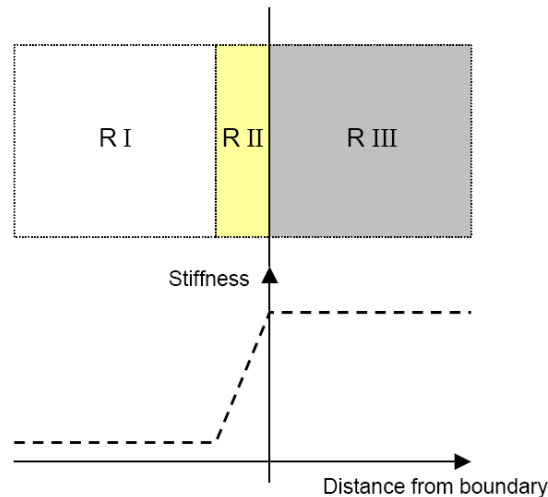


Figure 2 - Three region stiffness model (Harris, Davies and Jakopc 2004)

Additional problems with the Acrobot's design are that a force transducer is necessary to implement its control algorithm, significant impedance needs to be generated to effectively simulate a hard surface, and extra power must be generated to overcome the friction generated by the impedance in free space. These problems are costly to solve and limit the effectiveness of the design.

### 2.2.2 Cobot Concept

The Cobot (Continually Variable Transmission) concept is shown in Figure 3. Cobot attempts to implement a physical, mechanical hard constraint by steering a user in a direction tangent to the virtual surface. That is, a motor creates a frictional constraint along the virtual surface and instead of opposing motion perpendicular to the surface.



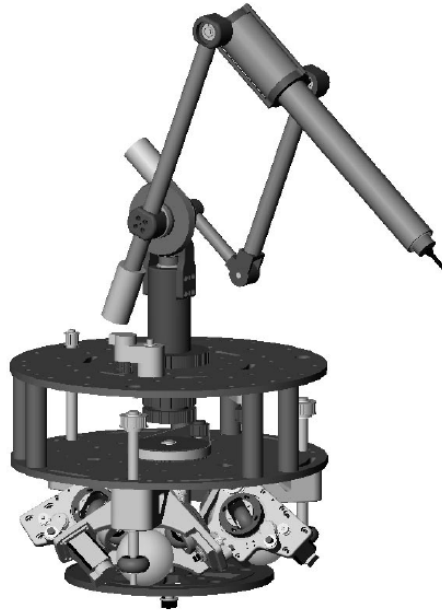


**Figure 3 - Cobot concept (Peshkin et al., 1996)**

The Cobot concept is advantageous because it uses real, physical constraints rather than motor impedances to emulate a hard surface. This eliminates two problems associated with the Acrobot: springiness at the hard surface and friction in free regions (motion becomes completely unconstrained). However, the nature of the design lends itself to several problems. Colgate et al. (1996) reported that inherent characteristics of the design caused two significant problems: the device hesitated when pushed from rest and the device steered the user off course when the virtual surface was approached at a steep angle causing surface penetration ranging from 10-40 mm. Moreover, users reported a small but noticeable delay in turning and steering the device, which prevents free motion away from the boundaries and is an additional cause of inadvertent penetration into restricted zones.

### **2.2.3 PADyC Concept**

The PADyC concept is shown in Figure 4. It is similar to the Cobot concept in that it uses mechanical means to emulate a virtual hard surface. The concept uses a “double freewheel and motor combination that allows passive motion within a set of dynamic constraints” (Troccaz and Delnondedieu 1996). Essentially, the concept consists of two shafts separated by a freewheel that rotate in opposite directions, where one shaft is driven and the other shaft is constrained by the

rotational speed of the driven shaft. When manipulators are attached to the shafts, the concept allows relative motion between the two arms to be controlled – this control can be used to implement a constraint for guided motion. The concept is advantageous because it uses passive constraint instead of active constraint, which makes it safer. However, the stiffness of the virtual surface has been found to be somewhat low (leading to penetration of the surface), and instability along the surface has also been reported.

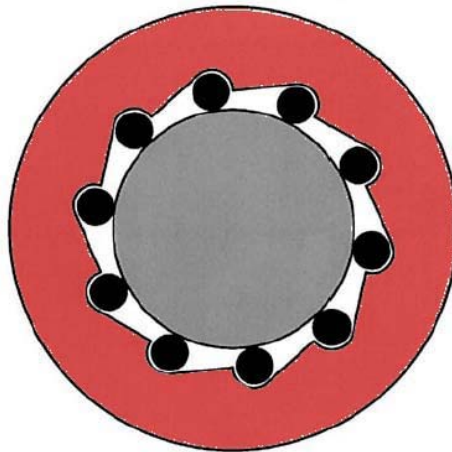


Figure 4 - PADyC freewheel concept (Troccaz 1996)

#### 2.2.4 PTER Dissipative Passive Concept

Another design that uses a mechanical means to control a user's motion is the PTER Dissipative Passive concept (Book et al., 1996), shown in Figure 5. The concept uses clutches and brakes to control the motion of a manipulator. In the figure, links 1 and 2 are connected by a coincident axis and their relative motion is controlled by the clutch and brake system at its base. Similar to the PADyC concept, the constraint is implemented passively. However, the concept has not been proven to effectively implement a hard constraint. Research (Swanson and Book 2003) suggests that a hard feel could probably be achieved using this concept, but motion along the boundary would be volatile as the brakes engage and disengage between the two zones.

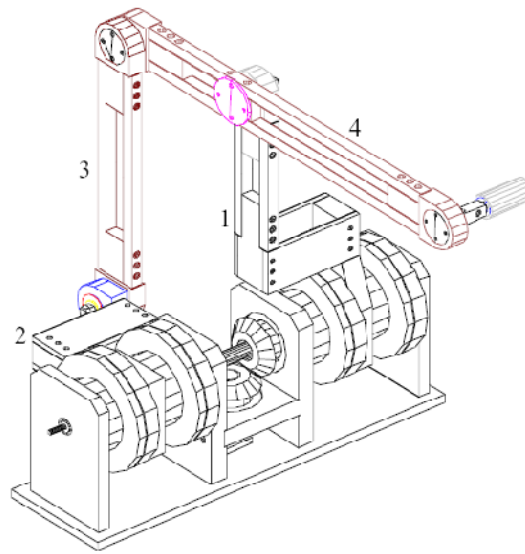


Figure 5 - PTER dissipative passive device (Book et al., 1996)

### 2.2.5 Mako Haptic Guidance System Concept

The final commercial technology discussed in this report is the Mako haptic guidance system shown in Figure 6. The system is a force-feedback haptic arm that is used to control cutting within a small incision. However, the system differs slightly from the other systems in that it does not automatically adjust to emulate a virtual hard surface during surgery but instead sets up a cutting guide based on a surgeon's preoperative plans. Although extremely flexible and versatile, its drawbacks are that it does not always create enough mechanical rigidity and that it uses motor impedance to create a hard surface in a fashion similar to the Acrobot (Hung 2008).



**Figure 6 - Mako haptic guidance system (photo courtesy of Mako Surgical Corp.)**

### **2.3 Previous Technology Developed for Praxim**

The Praxiteles robot (Figure 7) developed by Dr. Christopher Plaskos of Praxim effectively implemented haptic hard constraints but was limited to planar cuts. As such, Hungr's research focused on the implementation of a new two-dimensional haptic technique – Dynamic Physical Constraint. His approach is briefly described here to provide background for the differences between his design and the design presented in this report. Moreover, the reasons for several of the problems he encountered are examined; how these problems are resolved or mitigated are discussed in Section 4.2.3.

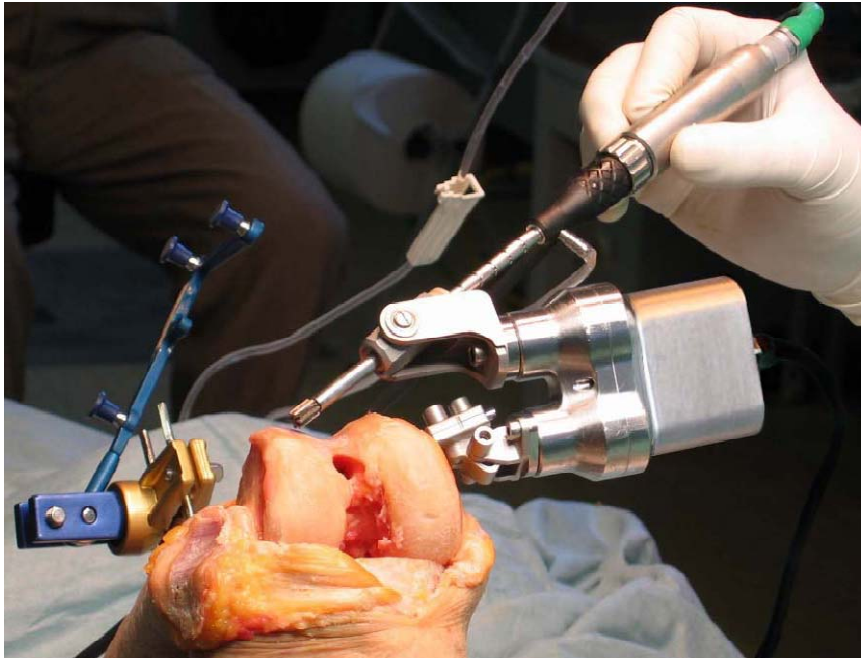


**Figure 7 - Original Praxiteles model (photo courtesy of Christopher Plaskos)**

### **2.3.1 Description of Hungr's Prototype**

Hungr's prototype (Figure 8) was designed to fit the Praxiteles' architecture and used an approach consisting of several links and constraints to realistically emulate a curvilinear hard surface while allowing the user to smoothly trace along the surface and have complete freedom away from the surface. The concept works similar to a doorstop in that the user can move the tool freely but is prevented from penetrating specific regions because of a physical barrier. In Figure 8, Link 1 is rigidly fixed to a flat surface and can rotate freely. Link 2 can also rotate freely but is constrained by the physical constraint driven by the motor.

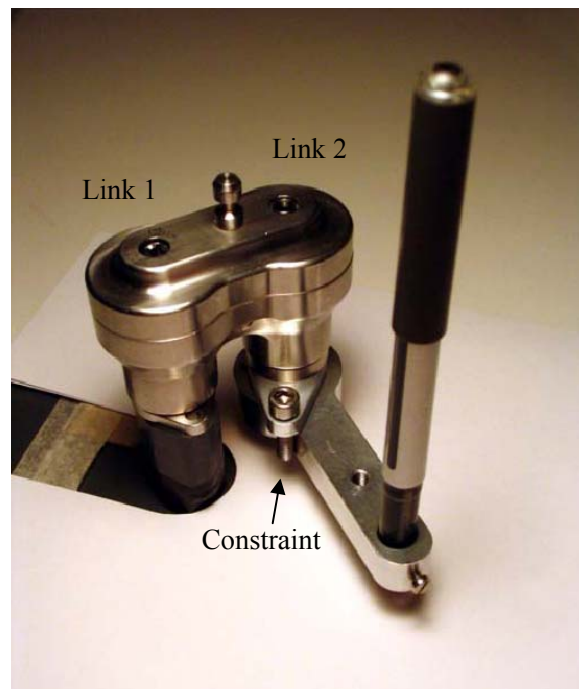


**Figure 8 - Hungr's haptic feedback prototype (2008)**

Two brushless DC servomotors (Faulhaber BL 2036B) with linear Hall sensors drive the system: the driving motor is connected to the constraint with a harmonic drive and the second motor is used only for its Hall sensor to measure the constraint's position. In addition, two motion controllers (Faulhaber MCBL 3006 S) connect the motors to a computer with a serial connection. A block diagram of the system is shown in Figure 9 (Hungr 2008).

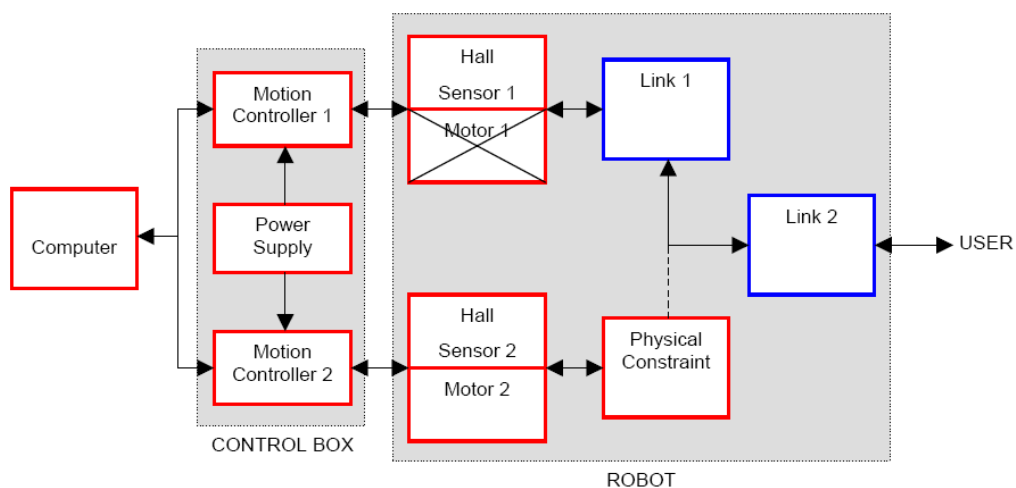


**Figure 9 - Block diagram of Hungr's prototype (2008)**

The user moves the end effector connected to Link 2 and the Hall sensors track the position of Links 1 and 2. This information is continuously sent through Motor Controller 1 to the computer and an algorithm on the computer developed by Hungr decides where the physical constraint needs to be to emulate the desired virtual surface. The computer sends the information back to the motor using Motor Controller 2 and the motor moves the physical constraint accordingly. A detailed description of the control program and details of the electronic components used is provided in Hungr's thesis entitled "Haptic Emulation of Hard Surfaces with Applications to Orthopaedic Surgery".

### **2.3.2 Identified Problems**

Initial prototype testing verified the concept's design, and users from experimental trials reported that the tool realistically emulated a hard surface and was smooth to operate. However, the prototype exhibited several characteristics that require resolution: lateral deflection, hysteresis and instability in certain situations.

When pushed towards the physical constraint, users reported that the manipulator laterally deflected due to a moment created around the robot's base. Lateral deflection was especially pronounced when the line connecting the end effector and the attachment point was close to parallel with the virtual surface and when the moment arm of the applied force was increased. The same behaviour arose when the manipulator was pushed along the hard constraint in certain directions – a "sticky" feel was reported by users. These issues are inherent with the two-link manipulator concept that was selected. The simplest solution is to carefully choose the robot's mounting position relative to where the work takes place. Based on this, the link lengths can be carefully chosen to match the kind of work that will normally take place. Another more comprehensive solution may be to use a different concept for tracking the tool's motion.

Hungr's prototype also exhibited hysteresis when subjected to quick motions of the manipulator along the physical constraint boundary. This was believed to be caused by the system's inability to update the constraint's position quickly enough. The delay in update speed was primarily caused by the response time of the motor and the control system design. The motor response time issue can be solved by using a higher quality motor and smaller gear ratio. The control

system design, likely the more significant problem, requires a more efficient approach than using serial communication between a PC and motor controllers with Hall sensors as the only position sensors. A comprehensive solution is proposed in Section 5.3.

In certain linkage configurations the linkage orientation led to instability, which caused the physical constraint position to quickly fluctuate. In some cases, this resulted in significant penetration into the virtual surface. This problem is also a function of poor system response time and an inefficient control strategy. Potential solutions include using more encoders to provide more information about the end effectors exact position and by using high resolution digital encoders instead of Hall sensors.

Hungr's research resolved many of the issues with other commercial haptic emulation technologies, but still suffered from several significant behavioural issues. The remainder of this project discusses how these issues were mitigated in order to design a physical prototype to emulate virtual, three-dimensional hard surfaces. Throughout the design and experimentation stages of this project, limitations in the current haptic emulation technology were discussed and addressed by optimizing and refining several design components including manipulator tracking, control strategy, and system architecture, among others.



### **3. Functional Requirements**

The objective of this project was to design a prototype capable of emulating a three-dimensional virtual hard surface. The features and drawbacks of the existing technology presented in Section 2 were used to develop a comprehensive set of functional requirements; the ultimate goal for the project was to successfully emulate hard surfaces while eliminating the behavioural issues associated with the previous technology. Because this project was originally being developed for Praxim, Plaskos' and Hungr's work was used as the foundation for the functional requirements. However, additional requirements were added and other requirements were refined to suit the needs of this project. The project scope, design objectives and evaluation criteria for the functional requirements are presented here.

#### **3.1 Project Scope**

The reason for developing a hard surface emulation device is to be able to eventually apply the technology to orthopaedic surgery (particularly knee arthroscopy). The purpose of designing such a device is to reduce the duration – and therefore cost – of a typical knee surgery, minimize bone and tissue removal to optimize recovery time, and allow the surgeon to safely and efficiently create complex shapes that would not be possible without computer assistance. This project, however, was a proof-of-concept prototype loosely based on Hungr's work. As such, the testing the prototype in a medical context was not within the scope of the project. Instead, the scope of this project was limited to successfully implementing haptic feedback in three-dimensions while resolving issues noted in Hungr's research. The project was divided into four main components: mechanical, electrical, controls and algorithm. The scope of the mechanical design was to design a manipulator capable of freely moving in three dimensions and to design a system to impede the manipulator from moving past a virtual surface. The scope of the electrical design was to select components (e.g. encoders) to integrate with the mechanical design to provide input to the controls system. The scope of the control system was to redesign Hungr's system and algorithm to provide better response time by using a mechatronics approach. Finally, the scope of the algorithm design was to create an algorithm capable of defining three-dimensional virtual surfaces.

### 3.2 Design Objectives

Existing commercial technologies and Hungr's research have significantly advanced the haptic surface emulation field. In particular, the results from previous work have provided information about the design constraints that should be used to create an ideal hard surface emulation device. Hungr listed the following five design objectives for hard surface emulation: realistic surface collision, realistic surface rigidity, unrestricted surface departure, smooth and precise surface tracing and unimpeded motion freedom away from the surface (2008). Each objective is briefly described here, and the quantitative criteria developed to evaluate the objectives are discussed in Section 3.3.

**Realistic surface collision:** the virtual surface should feel like a physical surface and allow minimal or no penetration of the surface when a tool hits the surface with any velocity or force. Realistic surface collision is critical for hard surface emulation because it provides user with confidence that the virtual surface is sufficiently rigid to withstand impact.

**Realistic surface rigidity:** the virtual surface should be sufficiently rigid to not allow any penetration when a constant force is applied. That is, the surface should not "give" or feel "springy" when a user presses against the surface. This is particularly important for surgical applications because milling a bone requires that the surgeon apply a significant amount of sustained force against the surface.

**Unrestricted surface departure:** the user should not feel any stickiness or impulse when a tool is pulled away from the virtual surface. The user should be able to freely move away from the surface regardless of the position, velocity or acceleration of the tool. This is important because any stickiness or impulse could compromise the efficiency and safety of a surgical operation.

**Smooth and precise surface tracing:** the user should be able to smoothly trace along the virtual surface without any stickiness, instability, hysteresis or penetration of the surface. This is one of the most important design objectives because it allows the user to create a smooth virtual surface in an efficient manner.

Unimpeded motion freedom away from the surface: the user should be able to move completely freely away from the virtual surface. That is, there should be no friction or impulse forces away from the surface and the user should feel that the haptic emulation device is non-existent. This is important because it allows the user to feel that system is working with him and is a natural extension of his arm.

Each of the design objectives described here are relatively qualitative, but a properly engineered design requires both qualitative and quantitative evaluation criteria. As such, quantification of these objectives in the context of the design presented in this report is provided in Section 3.3.

### 3.3 Evaluation Criteria

The goals for this project were to resolve the issues associated with Hungr's prototype (lateral deflection, reverse stickiness, hysteresis and instability) and to add a third dimension of motion. As such, a comprehensive list of evaluation criteria was created to address the issues for the scope of a three-dimensional prototype. Table 2 lists the functional requirements and evaluation criteria developed based on a combination of the design objectives presented in Section 3.2, the behavioural issues identified by Hungr, and several other identified objectives.

**Table 2 – Functional requirements and evaluation criteria**

<b>Requirement</b>	<b>Qualitative constraint</b>	<b>Quantitative constraint</b>
Surface rigidity	End user feels that he is contacting an actual hard surface in a collision and when applying sustained force.	Surface rigidity > 10 kN/m (see Section 2.1)
Range of motion	Milling tool is able to produce curved and planar shapes in three-dimensions in a volume of a typical knee.	Dimensions: - 60 mm x 60 mm, viewing femur from the side (Hungr 2008)

		- Depth of 110 mm(Seedhom, et al. 1972)
Surface penetration	Haptic emulation device limits penetration into virtual surface in any orientation.	Surface penetration < 1 mm (from discussions with client)
Maximum allowable angular error	Sum of mechanical and electrical errors in linkages must not create a significant offset.	Offset in the front plane alignment < 3°
Reverse stickiness and lateral deflection	User feels no or minimal stickiness or lateral deflection over entire range of motion.	-
Response time	Response time is fast enough such that virtual surface is emulated without any significant delay.	-
Motor torque	Motor must provide enough torque to withstand expected force from surgeon's hand.	Expected maximum moment of 7.5 Nm (50 N at 15 cm, determined by experimentation with cutting force)
Angle of attack	User can adjust angle of attack without affecting hard surface emulation.	No restrictions on angle of attack

The remainder of this report focuses on the development and design of a prototype capable of emulating virtual hard surfaces in three-dimensions. A number of different concepts were generated to meet the evaluation criteria described above; concept generation is described in Section 4. Testing of the final prototype validated that the design met most of the functional

requirements; the design of the final prototype is described in Section 5 and the testing performed to validate the functional requirements and identify any areas for improvement is described in Section 6. Recommendations for future work are provided in Section 7.

## **4. Concept Generation and Evaluation**

A comprehensive selection process was used to systematically decide on a concept that met the project requirements. Two main iterations are discussed here: initial and detailed concept evaluation. The initial evaluation phase consisted of developing a number of different concepts that could meet the requirements without significant regard for feasibility, cost or manufacturability. Each concept was then evaluated against the requirements discussed in Section 3 and three designs were selected for further analysis because they were determined to be the most feasible. The detailed evaluation phase consisted of developing the three selected concepts and evaluating them in a more quantitative manner. A final concept was selected from the three concepts after performing detailed analysis on each of them. Detailed design decisions for the final concept are discussed in Section 5. Please refer to Figure 29 on page 38 for a diagram outlining link, axis and encoder numbers if necessary.

### **4.1 Initial Concept Evaluation**

An understanding of the geometry of the knee was required before any concept generation began. The part of the knee relevant to the design is where the femur joins the knee (the distal femur). It is a complex shape: it is rounded from the front to the back and from side to side and there is depression through the middle. Figure 10 shows a Solidworks model of the femur (left) and a simplified model (right).

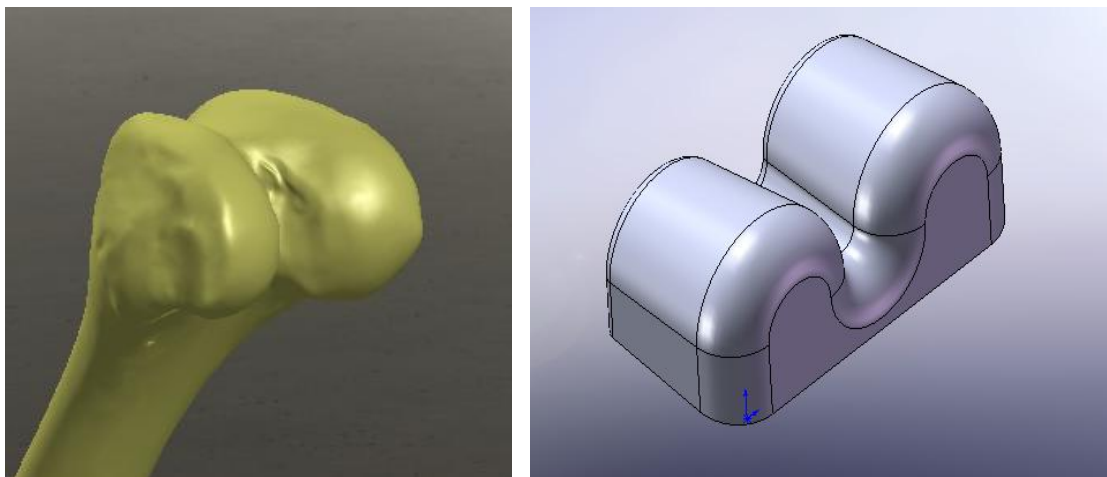


**Figure 10 - Distal femur (left); simplified model (right)**

A robot designed to mill the femur must

be able to reach every part of the bone with the cutting edge of the mill (either the side of a cylindrical mill or a range of angles with a ball mill). This requires operation in three-dimensional space with a minimum of three degrees of freedom. It is possible to work with up to six degrees of freedom; however, an effective design should be as simple and small as possible for ease of use.

There are two primary ways of creating motion: rotational joints and translational members. Any design using these requires three degrees of freedom with two possible ways (rotational or translational) of obtaining each degree of freedom. There are eight permutations that can create a device with three “links” that can be used to move in three-dimensional space. A summary of the combinations is provided in Table 3.

**Table 3 - Permutations for three-dimensional motion with three links**

<b>Permutation</b>	<b>Link 1</b>	<b>Link 2</b>	<b>Link 3</b>
1	Linear	Linear	Linear
2	Linear	Rotational	Linear
3	Linear	Linear	Rotational
4	Linear	Rotational	Rotational
5	Rotational	Linear	Linear
6	Rotational	Rotational	Linear
7	Rotational	Linear	Rotational
8	Rotational	Rotational	Rotational

The permutations presented above were used to develop rudimentary concepts for the mechanical design of a prototype. For the purposes of this project, Link 1 is connected to the base (which is connected to the knee) and Link 3 is connected to the end effector. Moreover, for the remainder of this report, Axis 1 refers to the axis of rotation around the base and Axis 2 refers to the axis of rotation between Link 1 and Link 2. In order to visualize how all of these

combinations of joints would allow for three-dimensional motion, drawings were made and K’NEX models were built where possible. A sample K’NEX model is shown in Figure 11.



**Figure 11 - Sample K’NEX prototype**

Once the motion of each potential device was known, a preliminary evaluation of each permutation was done. The evaluation of each permutation is shown in Table 4 as a Pugh chart. Permutation 6 was used as the permutation to compare the other ones against because it seemed to be a fairly standard design.

**Table 4 - Evaluation of permutations**

Criteria	Permutation							
	1	2	3	4	5	6	7	8
Weight minimization	-1	0	-1	1	0	0	1	0
Workspace visibility	-1	-1	-1	-1	-1	0	-1	0
Surrounding tissue interference	-1	0	0	0	0	0	0	0
Manoeuvrability	-1	0	-1	1	0	0	-1	-1
Mechanical simplicity	1	-1	-1	0	1	0	-1	0
# of sensors (more than four is worse)	0	-1	0	-1	0	0	0	0
# of stoppers (more than one is worse)	0	-1	0	-1	0	0	0	0
<b>Total</b>	-3	-4	-4	-1	0	0	-2	-1

<b>Rank</b>	<b>6</b>	<b>7</b>	<b>8</b>	<b>3</b>	<b>1</b>	<b>1</b>	<b>5</b>	<b>3</b>
-------------	----------	----------	----------	----------	----------	----------	----------	----------

This exercise demonstrated that having linear movement come from the base is impractical for most situations. It involves anchoring a rod to the bone to allow for linear translation of the rest of the device. Such a rod would be relatively large in comparison to the size of the knee to allow the mill to access the entire knee. The rod would have to be placed in the front of the surgeon's workspace, which is why the linear base scored poorly in workspace visibility. Rotational joints have the advantage of being simple and easy to manoeuvre. However, when directly attached to the mill, rotational joints can lead to mill angles that are undesirable. They can also limit the ability of the tool to cut on the side opposite to the where it is attached to the bone and within the valley of the knee, as illustrated in Figure 12. As such, the analysis suggests that the best designs have rotational bases with translational members attached to the end effector.

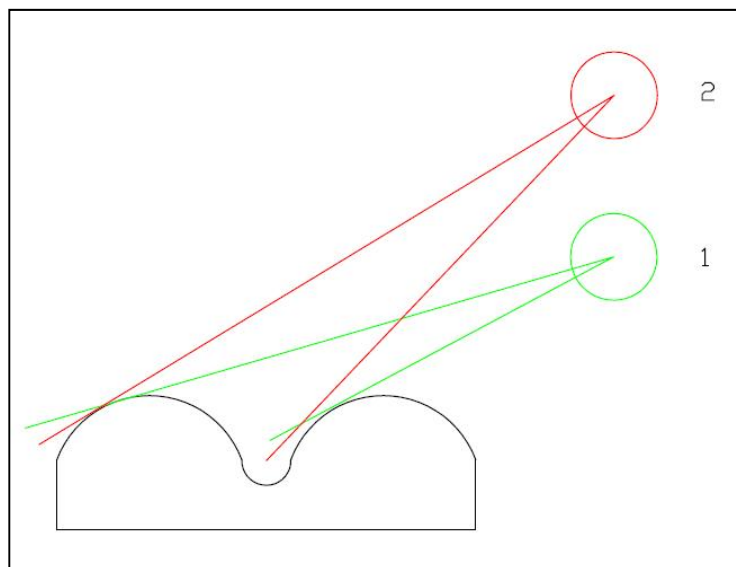


**Figure 12 - Angle of attack**

The evaluation suggested that permutations 5 and 6 were the best for a three-dimensional design. Three preliminary designs were developed based on these permutations. The first design, shown in Figure 13, consisted of a rotational base with two translational members.



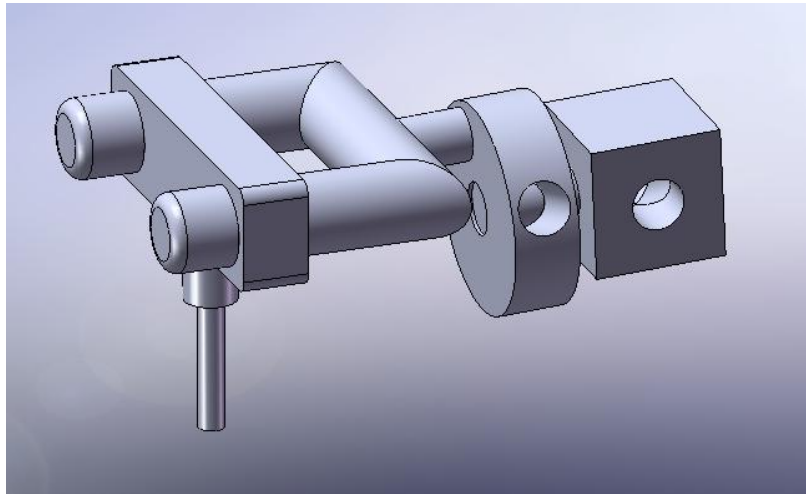


**Figure 13 - Rotational base with two linear sliders**

The second design, shown in Figure 14, consisted of a rotational base attached to another rotational joint and a translational member. The end effector was oriented perpendicular to the translational member.

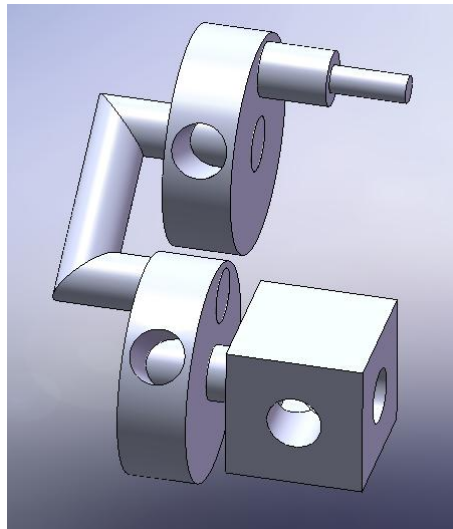


**Figure 14 - Two rotational joints with a linear slider**

The third design, shown in Figure 15, consisted of a ball joint that allowed for rotational motion in two directions and a translational member that was attached to the ball.

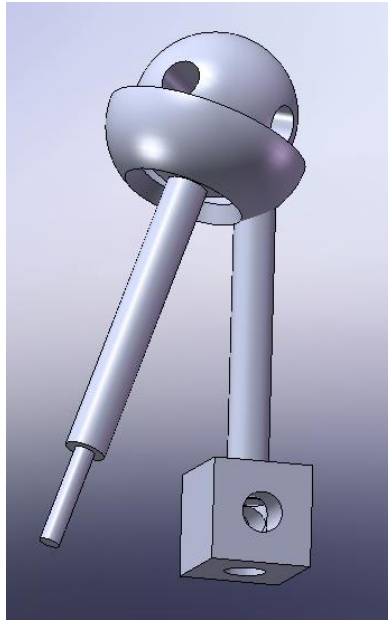


**Figure 15 - Ball joint with a linear slider**

The three rudimentary concepts described above were then developed into slightly more detailed designs for further analysis. Figure 16, Figure 17, and Figure 18 show the refined designs. These designs were used as the foundation for the detailed designs discussed in Section 4.2.

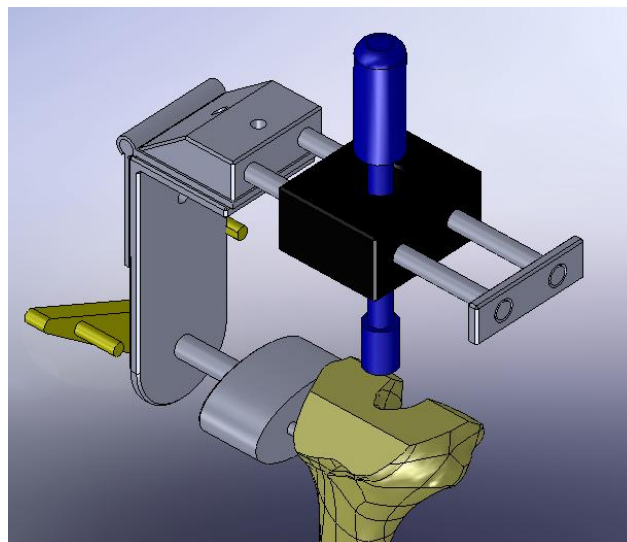


**Figure 16 - More detailed rotational base with two linear sliders**

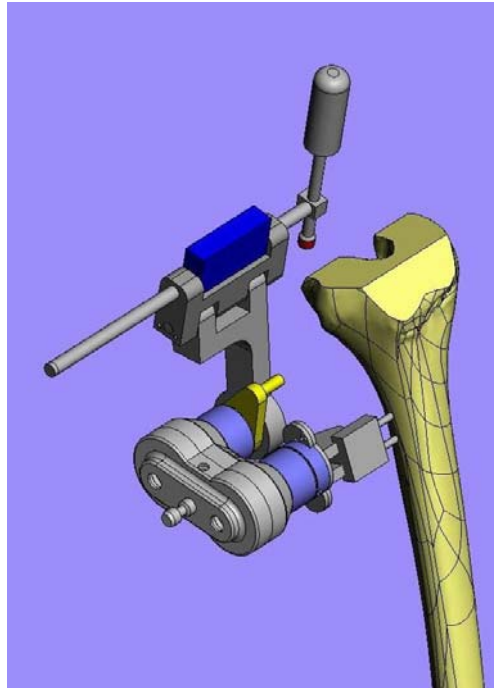


**Figure 17 - More detailed two rotational joints with a linear slider**

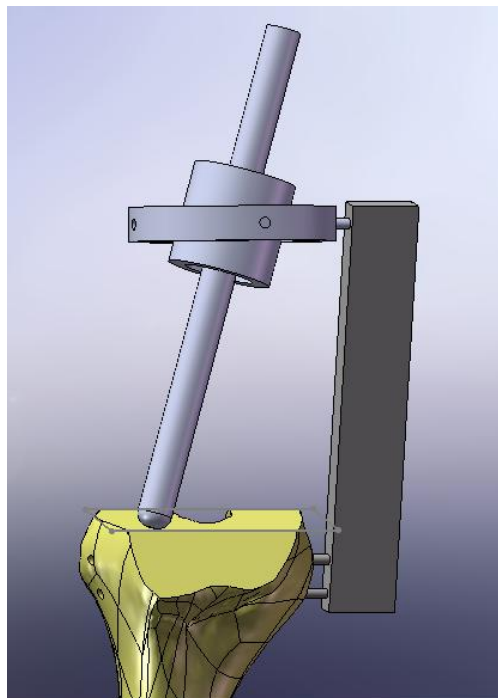


**Figure 18 - More detailed ball joint with a linear slider**

## 4.2 Detailed Concept Evaluation

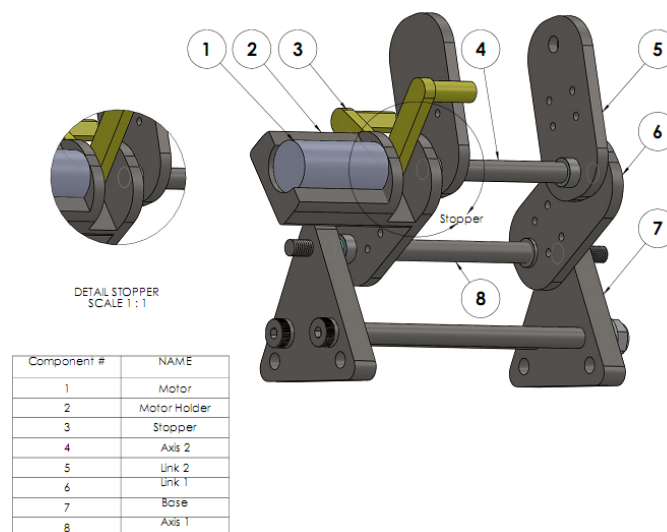
The second iteration in the concept evaluation stage involved investigating specific aspects of the design in detail. In particular, the rotational joints, linear bearing and controls architecture were examined. A number of concepts were developed for each item and compared to decide on the best design for the final prototype.

### 4.2.1 Rotational Joints Concepts

There were three main concepts that were developed for the two rotational joints. Three designs were examined because attaching an encoder between Link 1 and Link 2 while keeping the motor and stopper assembly concentric with Axis 2 was a complex and crucial component of the design. The rotational joints had to be designed properly to make the structure rigid – any play in the joints would make achieving sub-millimetric accuracy difficult. In general, the rotational joints were generated using criteria such as minimum constraint design, rigidity, manufacturability, usability, and minimal complexity.

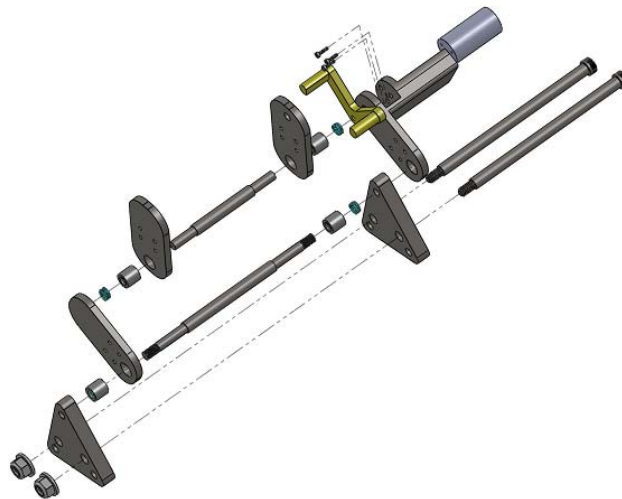
#### *Design 1 – Sheet Metal*

Figure 19 shows the sheet metal concept that was developed for the rotational joints and identifies which components correspond to which axes and links.



**Figure 19 - Sheet metal design**

The sheet metal concept was developed because it would be easy to machine and manufacture. Moreover, its simple design would be ideal for reducing size and weight. The entire assembly is connected to a mountable triangular base through Axis 1. The motor rests on a holder that is attached to Link 1. The stopper is secured on the motor shaft and is used as a guide to restrict the motion of Link 2. Axis 2 connects Links 1 and 2. The device shown does not include Link 3 (at the free end of Link 2) which would enable movement of the apparatus in a third dimension. The addition of this linear link is discussed in Section 4.2.2. All the links are not driven by a motor and would be freely controlled by a surgeon. The V-shaped motor stopper is secured on the motor shaft and is used as a guide to restrict the motion of Link 2. There are a total of four flanged-bearings used in the design (two on each axis). The bearings are clipped to the link with a tight fit. Disk springs are used to keep the components intact on each link and reduce the possible external noise. Figure 20 shows an exploded view of the design.



**Figure 20 - Exploded view of sheet metal design**

The concept is expected to occupy a total volume of  $148 \text{ cm}^3$  and has a mass of just over 1 kg excluding the third link, encoders, and the tool holder.

### ***Design 2 - Thrust Bearing***

The thrust bearing design is shown in Figure 21.

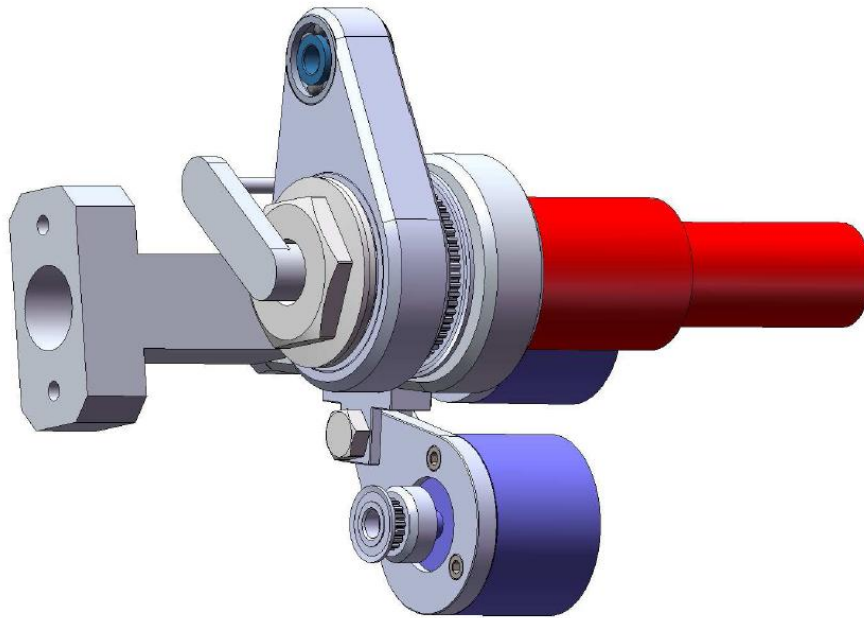


**Figure 21 - Thrust bearing design**

The thrust bearing design is unique because the motor shaft is connected to the stopper through the linkages. This allows for the stopper to have 360 degrees of motion, and also gives Link 2 the potential to rotate 360 degrees depending on the length of Link 1. The links are held together with a 20 mm diameter bolt drilled through its centre to allow the motor shaft to penetrate through. The relative motion of Link 1 to Link 2 is tracked by an encoder mounted beside Axis 2. This encoder is driven by a timing belt that moves with Link 2. Using a timing belt to drive the second encoder was considered one of the weaker points of this design; it was unknown how this would perform in actual testing, particularly in a surgical environment.

To achieve the required rigidity in the X-, Y-, and Z-directions, an angular contact bearing was used in conjunction with a thrust bearing. Figure 22 shows an angular contact bearing located within Link 2.

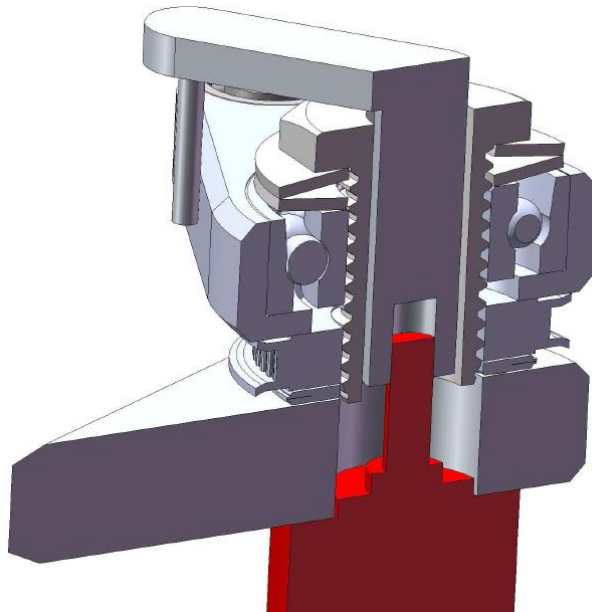


**Figure 22 - Three-dimensional cutaway of thrust bearing design**

There is also a needle bearing between the face of Link 1 and the timing belt pulley wheel. This is shown in the force diagram Figure 23. This arrangement of bearings satisfies minimum constraint design theory because Link 2 is constrained from moving up and down by the angular contact bearing and from moving left or right by both bearings combined. The combination of bearings also leads to the linkage being only allowed to rotate about one axis. The total weight of this design is 633 g.

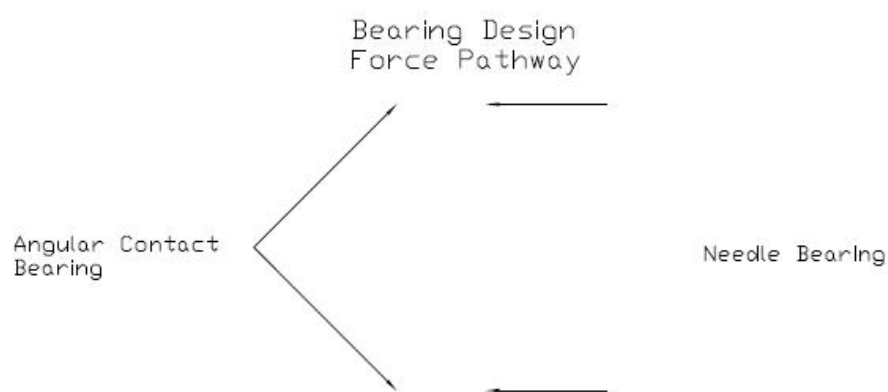


**Figure 23 - Bearing design considerations**

Figure 24 shows an exploded view of the thrust bearing design. The encoders are highlighted in blue and the motor and gearbox combination is highlighted in red. The critical components located at Joint 2 (as numbered in the figure) are illustrated in Figure 25. From left to right, the components are: Link 1, thrust bearing, main timing belt pulley, Link 2, angular contact bearing, and two spring washers located on the screw and the stopper.

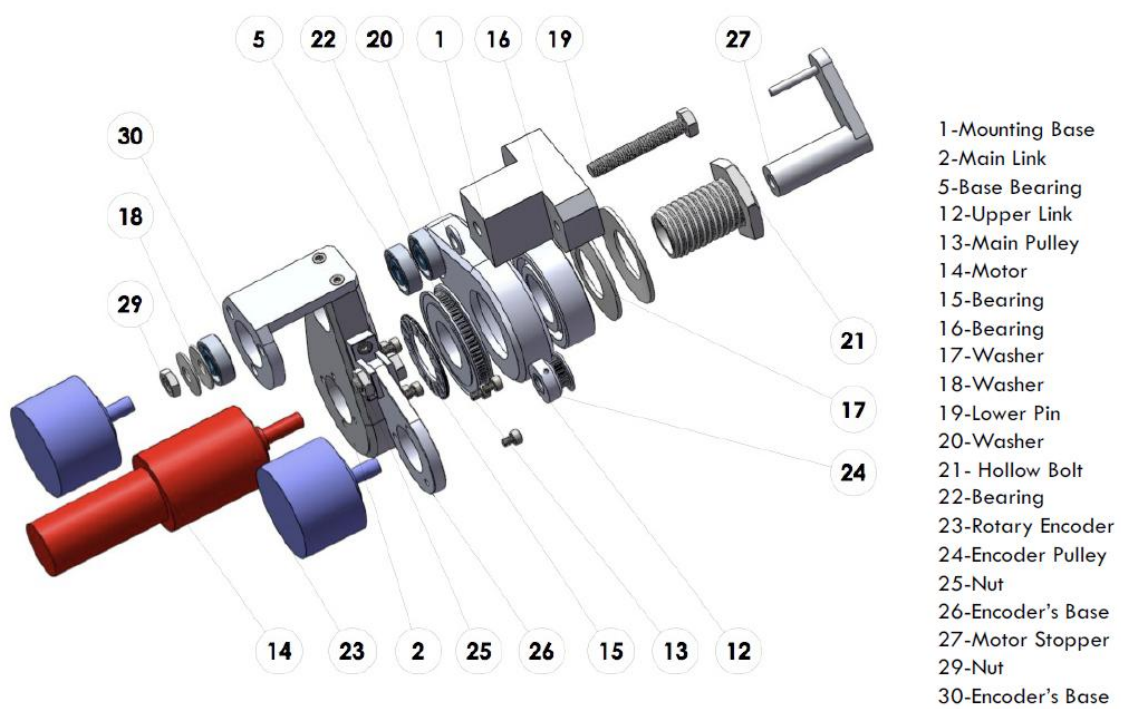


Figure 24 - Exploded view of thrust bearing design

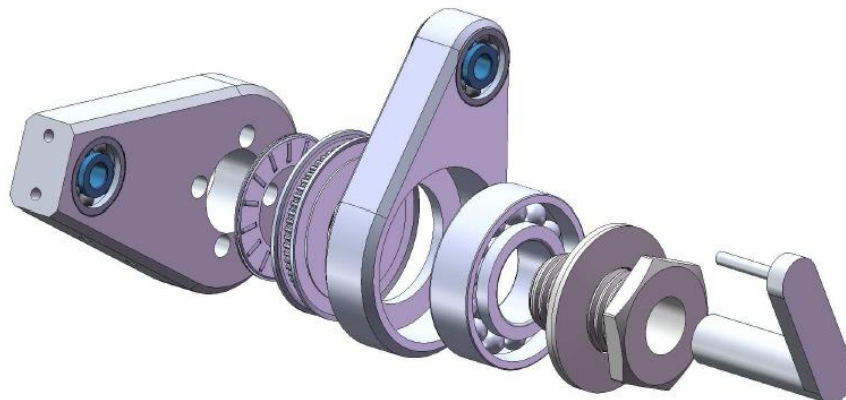
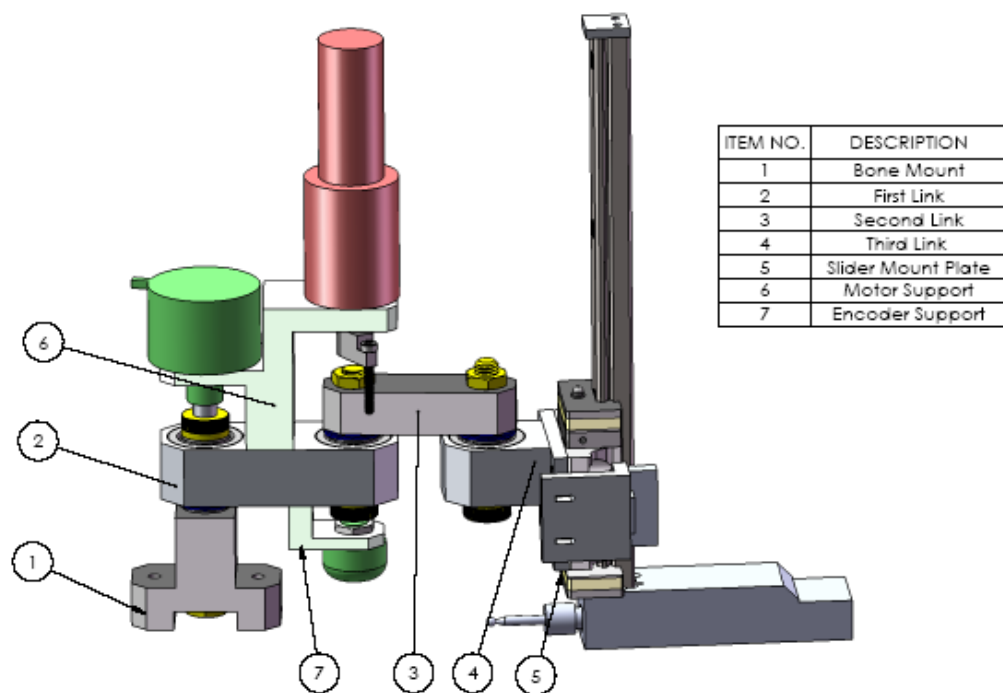


Figure 25 - Exploded view of critical parts at joint 2



### ***Design 3 – Angular Contact Bearings***

In this concept the motor and encoders are offset from the two links, which allows easier access to components and makes assembly of the device easier. This concept consists of two links designed to produce rotational motion and support brackets mounted on the primary link to support the motor and encoders. Figure 26 shows an overall view of the concept.



**Figure 26 - Angular contact bearings concept**

This approach uses two rotational joints and one linear slider in order to access the full workspace, which was determined to be the best method of doing so in Section 4.1. Two pairs of angular contact bearings are used to allow for freedom of motion in a plane. These bearings are located in pairs inside Link 1 and Link 3. The orientation of the bearings supports all axial and radial forces and provides rigid rotational motion on the linear plane.

The first link and bone mount are connected through a shaft that sits inside Link 1. The shaft allows for free rotation of Link 1 while the shaft remains stationary with respect to the bone mount. The second shaft connects Link 1 and Link 2. This shaft is fixed with respect to Link 2

and rotates freely in Link 1. The second pair of angular contact bearings sits around this shaft and inside Link 1.

The motor support is mounted directly onto the first link; it holds the motor and the first axis encoder. This part is designed to allow the first encoder to rotate about Axis 1 and the motor to rotate about Axis 2 without causing any interference for the rotation of the axes and to avoid too many axes in the same location. Similarly, the encoder support allows the encoder on Axis 2 to sit at an offset and rotate around Axis 2.

This concept allows for easy assembly and disassembly of mechanical links and is also relatively easy to manufacture. The concept provides a number of different orientations for installation of the two links, encoders and motor. At 625 g, this concept is the lightest out of all three designs.

### ***Rotational Joint Design Selection***

The choice of which rotational linkage design to use was one of the most important mechanical design decisions. Design 1, the sheet metal design, was eliminated fairly quickly. It was eliminated because it was more complicated, larger and heavier. With a mass of 1 kg, the sheet metal design outweighed the other two concepts by 400 g. It stuck out about 25 cm from the knee from the base to the end of the motor because of its parallel plate design with encoders mounted between the sheet metal sides. In comparison, Design 2, the thrust bearing design, stuck out 17 cm, and Design 3, the angular contact bearings design, stuck out 20 cm. Another concern with the sheet metal design was that it would be quite complicated to assemble and disassemble, and difficult to tolerance correctly. As such, the sheet metal design was eliminated and the thrust bearing and angular contact bearing designs were focused on.

The second and third designs were developed in more detail than the first design. They were about the same weight and size, but were differentiated by how they dealt with the concentration of parts at Axis 2. Ultimately, **Design 3** was chosen as the design for the final prototype because of several possible problems with Design 2.

Each design could effectively cover the plane that was required and each design was theoretically rigid. Design 2 was more compact than Design 3; however, it was heavier because of the large steel angular contact bearing. A significant potential problem was associated with the fact that the encoder attached to Axis 2 was driven by a belt drive. This was a concern for the client as he was unsure how this would perform in a surgical environment. Another concern was how well the bearing setup would constrain motion. Although it theoretically appeared to work, an example with that setup could not be found so there was uncertainty associated with the design. Design 3 could achieve all that Design 2 could with less uncertainty, so it was decided that Design 3 should be developed into the final prototype.

#### 4.2.2 Linear Bearing Concepts

There were two main concepts considered for the linear slide, both of which involved using linear bearings for smooth accurate motion. Design 1 is shown in Figure 27 and Design 2 is presented in Figure 28.

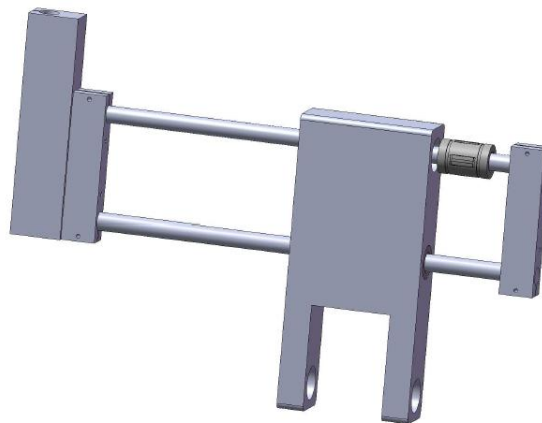


**Figure 27 - Design 1 for the linear bearing**

Design 1 involves using four linear bearings that are mounted in an aluminum housing. The linear bearing can be seen in Figure 27 at the top right side on the rail. There are two  $\frac{1}{4}$ " rods that slide back and forth to provide motion in one direction. This design would be almost completely fabricated; only the linear bearings and the rods would be purchased. The second rod is required to prevent the rod from rotating. In practice, this design would be very heavy because

the rods and bearings are made of steel. Furthermore, the design is relatively complicated because the rods have to be aligned perfectly to move smoothly back and forth.



**Figure 28 - Design 2 for the linear bearing**

Design 2 is a linear bearing slider that is purchased as a prefabricated unit. It has fixed preloads applied by the manufacturer to compensate for torque loads on the shaft. This unit is also heavy because the rail is made of steel.

### ***Linear Bearing Selection***

**Design 2**, the prefabricated assembly, was chosen to use in the final design for the linear slider. The reason for this is because Design 1 was more complicated and was dependent on very precise machining. While it was theoretically possible to achieve such machining precision, it was not known how well aligned the rails would have to be to slide freely. Another problem identified with Design 1 was that it was heavier than the prefabricated linear slider assembly. Moreover, previous experience with prefabricated linear slide assemblies confirmed that they performed well with almost zero deflection.

#### **4.2.3 Controls Architecture**

Two main alternatives were considered for the controls architecture. Both eliminated the need for a non-dedicated PC to perform any calculations in order to increase system response time. The first alternative, Design 1, was to use an embedded, dedicated xPC host-target system to accept inputs from the encoders, calculate the motor blocker position, and perform trajectory generation to control motor blocker position. All of the coding and debugging could be performed on a host computer and transferred to the xPC embedded target computer to control the motor. Fast response times would be attained by using CAN communication to transfer data instead of the slower RS-232 (serial) connection used in Hungr's prototype. This would require an additional

CAN communication card as well as a data acquisition board that would have to be purchased and installed on the xPC computers. The system would theoretically be easy to troubleshoot, but the cost for the system would be relatively high and the initial implementation would be time consuming.

The second alternative, Design 2, involved sending encoder signal inputs to microcontroller that computes the blocker position. The final blocker position would be sent by the microcontroller via CAN bus to a motor controller that controls the blocker position via a brushless DC motor. Both the microcontroller and the motor controller would be connected to a computer for programming and debugging purposes. This option seemed to have a lower cost than the xPC option and would be easier to setup, but would be significantly more difficult to design in detail.

**Design 2** was selected as the controller architecture, primarily because the uncertainty associated with its implementation was lower than Design 1. The detailed design of the system is presented in Section 5.3.1.

## 5. Design and Analysis

The design of the final prototype consists of four different types of design: mechanical, electrical, controls system and algorithm. The completed design is shown in Figure 29 with annotations describing the link, axis and encoder numbers referred to in this section. Each design type is presented separately in this section with a description of the components designed and justification for their selection.

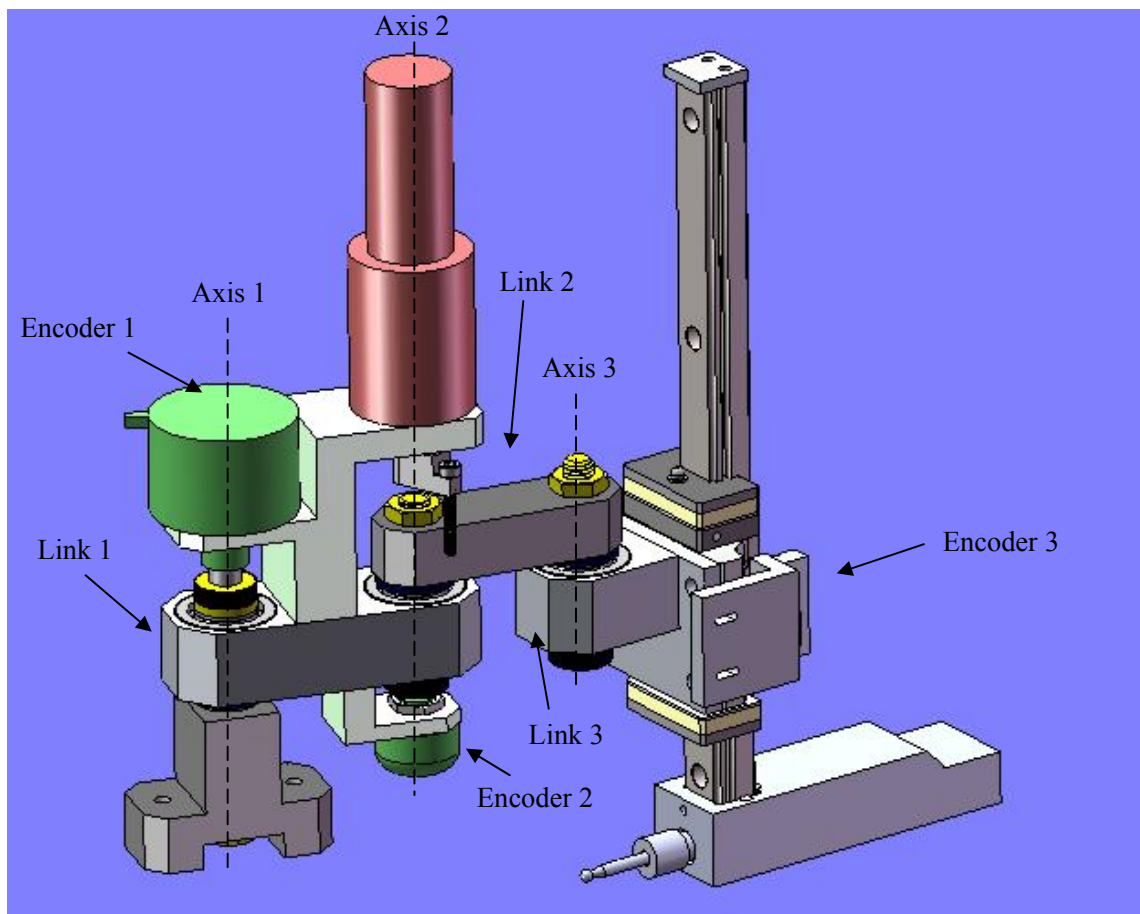


Figure 29 - Final design with axis, link and encoder numbers

### 5.1 Mechanical Design

The design objectives for the mechanical system were to maximize rigidity and minimize mass while designing components that would be easy to manufacture, assemble and use. This section outlines each part of the design and provides justification for why the part was chosen or how it

satisfies its function, separated into purchased and manufactured components. A mechanical deflection analysis is performed for critical parts that are subjected to load during operation. Deflections and stresses were expected to be very low because linkage sizes are relatively large compared to the modest loads expected for the design. The deflection analyses performed validated those expectations. In general, it would have been ideal to reduce the size of the bearings which would reduce the size of linkages and the overall size and weight, but budgetary constraints limited bearing selection. Simple parts (e.g. shoulder screws used as shafts) have been excluded from the following section. Full detail drawings for all relevant parts are provided in Appendix A, and all relevant data sheets are provided in Appendix B.

### 5.1.1 Purchased Components

This section describes components that were purchased directly from manufacturers or suppliers.

#### ***Angular Contact Bearings***

The orientation of the angular contact bearings is shown in Figure 30. This orientation is called “back-to-back”, as illustrated in Figure 31. With this orientation, force is applied to the inner race of the bearings and transferred through the bearing to the outer race and then through the linkage to the next bearing. The force diagram of this bearing setup is illustrated in Figure 32. When choosing the bearings the primary considerations were size, cost, sealing and loading. The speed rating of the bearing was not considered because the bearings were expected to be operated at very low velocities.

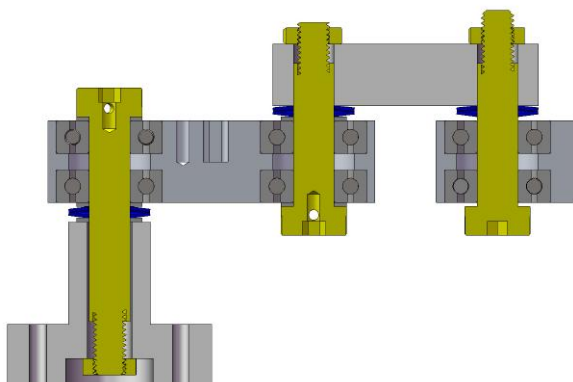


**Figure 30 - Angular contact bearings orientation**

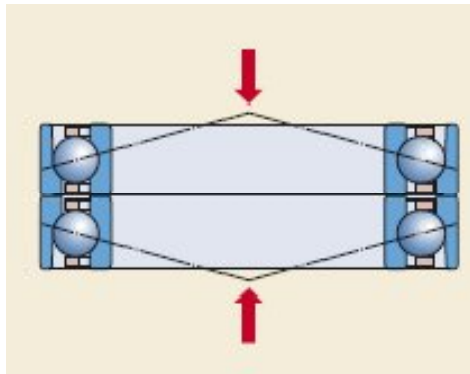


**Figure 31 - Back-to-back bearing orientation**

The bearings selected for the design are NSK general purpose, non-precision, open ball-bearings with  $15^\circ$  contact angle. The bearings are 26 mm O.D., 10 mm I.D., and 8 mm thickness. Ideally, smaller bearings would have been used, but smaller precision bearings were too expensive for the project's budget. The angular contact bearings that were purchased cost \$75 per pair – to move to the next size down would have cost \$300 per pair. Sealed bearings were also not selected because of cost. Bearings for a medical device such as this would be sealed to keep out any debris created during milling, but for the proof-of-concept prototype created non-sealed bearings were sufficient.

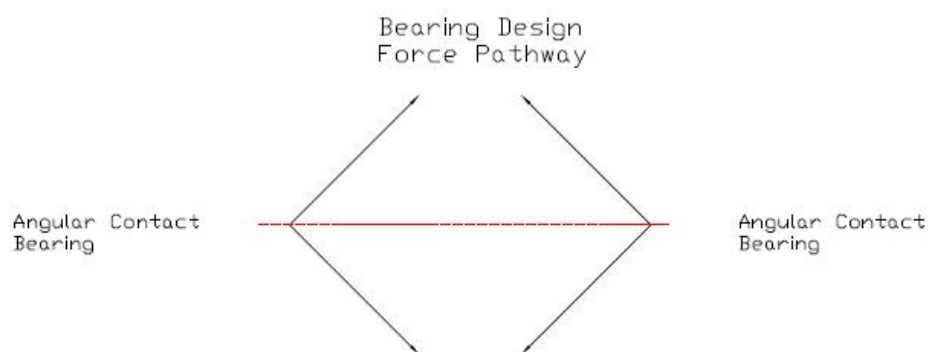


**Figure 32 - Force pathway**



### ***Linear Ball Bearing***

The linear ball bearing selected for the design is shown in Figure 33.

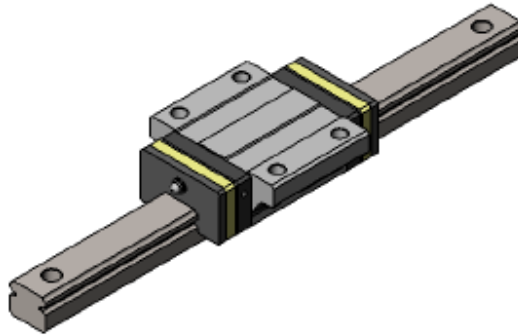


**Figure 33 - Linear ball bearing**

The linear ball bearing was sized based on a deflection calculation and the standard rail sizes provided by the manufacturer. Objectives for the ball bearing were for it to be light, have a bearing that could withstand a large moment and have a sliding rail with minimal friction. There is an inverse relationship between how much moment the bearing can withstand and how difficult the rail is to slide. Using manufacturer supplied datasheets, it was found that medium loading could withstand the experimentally determined required moment of 7.5 Nm (50 N force at 15 cm) while still sliding easily. Three different deflection calculations were done to size the rail. In particular, two calculations were performed by hand and one was done using finite element analysis (FEA), the results of which are presented in Figure 34. The hand deflection calculations were performed for a cantilever beam with a point force. The maximum length of the beam used was 15 cm. The second moment of area was calculated for a beam both with and without holes. The calculated deflections were 0.16 mm and 0.1 mm, respectively. The finite element software yielded a deflection of 0.15 mm. The linear bearing and rail selected for this project are NSK LS series size 15.

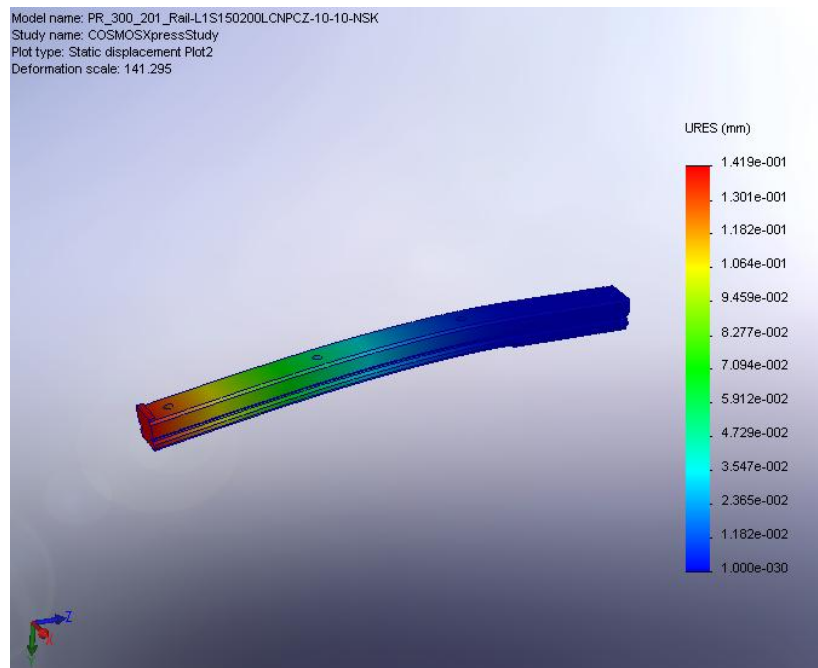


**Figure 34 - Linear ball bearing finite element analysis**

### ***Shafts***

Three shoulder screws were selected and used as the shafts attaching the linkages. Using shoulder screws as shafts significantly improved the manufacturing process. Also, the end shoulder and the thread of the bolt improved preloading and made constraining the shaft simpler. Assembly and disassembly of the device was much easier with the use of the shoulder screws.

### ***Spring Washers***

To create the required preload on the angular contact bearing a spring washer was included on all of the shafts. The spring washer was selected based on the preload recommended by the bearing manufacturers. The selected spring washers were ball bearing Belleville disk springs. The load rating of the spring washer is 51 N and the deflection at that load is 0.26 mm.

### 5.1.2 Manufactured Components

This section describes components that were designed and manufactured.

#### ***Bone Mount***

Figure 35 shows the component that was manufactured to mount the final prototype to the “bone” (a solid block of aluminum was used in place of bone for the scope of this project).

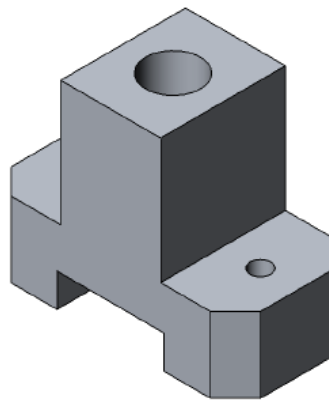


**Figure 35 - Bone mount**

The mount was designed as a temporary component to mount the final prototype onto custom designed platform for testing. The prototype was designed to allow the bone mount used by Praxim for the Praxiteles robot to replace this mount with only minor modifications. The two smaller holes are used to mount the robot onto the test platform. The centre hole is intended for the shaft of Axis 1. This hole was reamed with a very tight tolerance to allow the shaft to have full contact with the part and to avoid any backlash in the joint. As such, the shaft does not rotate with respect to the bone mount. The height of the bone mount was set to allow clearance for the encoder on Axis 2 and to place all components at a reasonable offset from the mounting surface. The slot on the bottom is indented for access to the nut of the shoulder screw.

### ***Link 1***

Link 1 is shown in Figure 36.

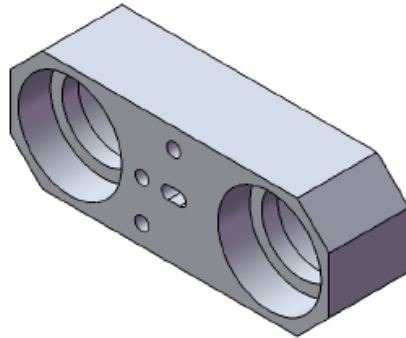


**Figure 36 - Link 1**

This link connects the bone mount to the rest of the assembly and acts as a mounting platform for the motor support and encoder support. The link was optimized to fit all of the bearings for Axis 1 and Axis 2 in order to minimize the number of CNC-machined parts. The overall dimensions of the device were selected based on the size of the bearing located inside the housing of the device. The centre-to-centre distance of the counter bores was set to 50 mm, which was based on Hungr's recommendations for optimizing the blocker positioning algorithm (2008). Finite element analysis was also performed on the device to ensure minimal deflection in the member. The results of the analysis are shown in Figure 37.

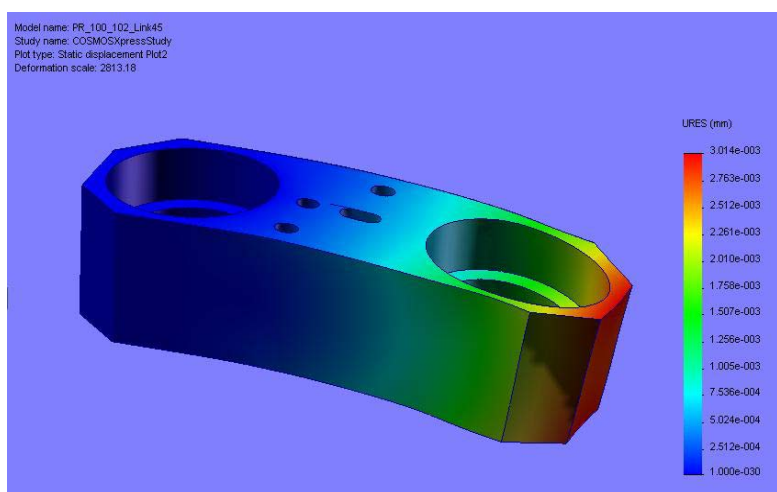


**Figure 37 - Link 1 finite element analysis**

Link 1 has four counter bores paired in two which act as housings for the angular contact bearings. Axis 1 runs through the first pair of bearings and then through the hole in the centre of the bone mount. The spacers and spring washer are located under these links and above the bone mount. The counter bores were machined with a tolerance of H7 to avoid any backlash or play in the assembly, and the bearings were force fit into the counter bores. The bearings are oriented back-to-back in order to provide maximum bi-directional thrust capability. The outer rings of the bearings sit on the shoulders in between the counter bores and the inner rings sit onto the shaft which runs between the two bearings. The preloading of the shaft compresses the ball bearing in between the two rings and eliminates any possible backlash in the bearings. This orientation allows the link to rotate freely about Axis 1 regardless of the type of load applied. The second set of bearings is force fit with the same orientation to allow the second shaft to rotate freely with respect to Link 1.

On the top side of the link a dowel pin hole and a slot were located to act as alignment features between the link and the motor support. These features correspond to the two dowel pin holes on the motor support in order to align the two components perfectly. In addition, the slot compensates for inaccuracies in the machining and constrains the two parts with the correct number of degrees of freedom.

On the opposite side of the link, the two countersunk through holes allow the motor support to be attached to the top face of this link using standard bolts. Moreover, the encoder support is mounted to the same face and aligned so that the encoder is in line with Axis 2.

### ***Link 2***

Link 2 is shown in Figure 38.

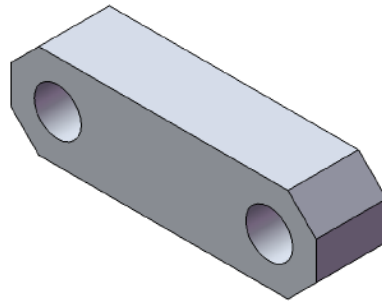


**Figure 38 - Link 2**

Link 2 is a block which connects Link 1 to the rest of the assembly. The block has two 10 mm holes which are 45 mm apart. The second and third shaft runs through these holes and is attached to Link 1 on one side and to Link 3 on the other. The second and third shafts are stationary with respect to this link, which can be achieved by proper preloading of the shoulder screws. In addition, two set screws on the back face of this link ensure that the shafts do not rotate with respect to these links.

The 45 mm distance in between the two axes was designed based on recommendations provided by Hungr (2008) to optimize the algorithm for the considered patterns. The height of the link was determined using finite element analysis and was designed to minimizing the size and deflection of the link. The results of the analysis are shown in Figure 39. The analysis confirms that the expected deflection of the link is minimal.

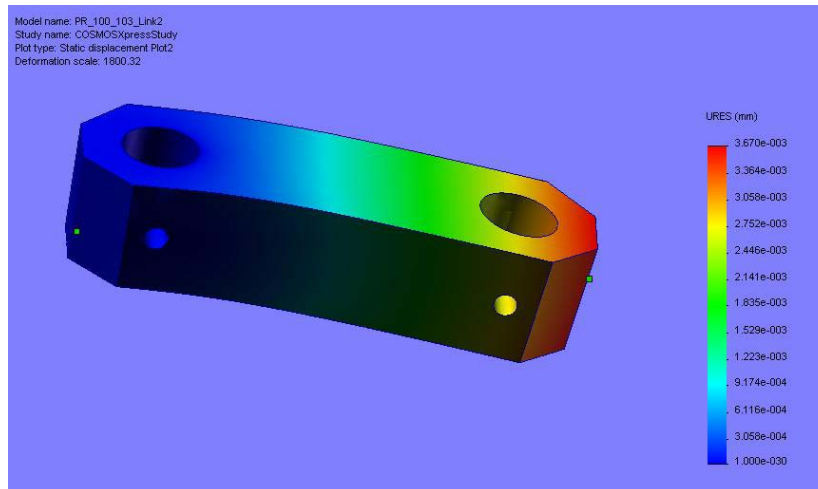


**Figure 39 - Link 2 finite element analysis**

### ***Link 3***

Link 3 is shown in Figure 40.

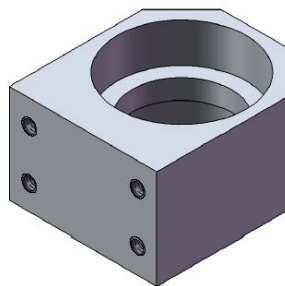


**Figure 40 - Link 3**

Link 3 is similar in design to Link 1. This link was designed to allow angle of attack freedom. The assembly is designed such that the end effector is always on the third axis of rotation. The link has two 26 mm counter bores which are designed to fit a pair of angular contact bearings. These bearings allow Link 3 and the linear ball bearing assembly to rotate freely with respect to Axis 3. The dimensions of the device were dictated by the size of the bearings and the required clearance for placement of four threaded holes attaching the link to the mounting plate. The angular contact bearings are oriented in the back-to-back configuration to provide maximum bi-directional thrust capability. The counter bores had a tolerance of H7 to remove any backlash in

the device and the bearings were force fit into the counter bores. This component was fabricated using a CNC machine.

### ***Motor and Encoder 1 Support***

The support for the motor and Encoder 1 is shown in Figure 41.

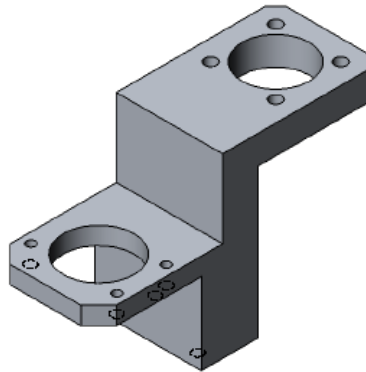


**Figure 41 - Motor and Encoder 1 support**

The motor support was designed to allow the motor and encoder to rotate on the same axis as the primary device axes. By doing this, the use of belts and pulleys to attach the motor and encoder was avoided. In addition, this design helped overcome space limitations due to having too many axes in the same location. Two dowel pin holes are located on the bottom face of the support to allow for accurate placement of the motor support with respect to Link 1. The through attachment holes on Link 1 allow attachment of the two components using bolts.

The height of the motor support was designed to allow clearance for placement of Link 2, a shoulder screw nut and the blocker on top of Link 1. The opening on the motor side of the link was optimized to allow full rotation of the stopper and to maximize the rotation angle of Link 2. Unfortunately, the large bearings selected limited the available range of motion of Link 2 to 240°. The use of smaller bearings in future designs could increase the range of motion of Link 2.

On the encoder side, the top opening was sized to allow for proper fitting of Encoder 1 in line with the first axis. The height of the mount location was set to allow easy assembly of the device and preloading of Axis 1 while keeping the encoder as close as possible to the shoulder screw.



### ***Encoder 2 Support***

The support for Encoder 2 is shown in Figure 42.

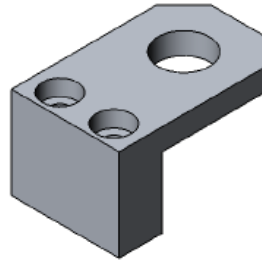


**Figure 42 - Encoder 2 support**

This bracket is mounted on the opposite side of the motor support and allows attachment of the encoder on the same axis. The height of the bracket was minimized to allow for the head of the shoulder screw and the shaft of the encoder. The mounting holes were over sized by a millimetre to prevent over constraining the shaft. The encoder was selected such that it would allow for minor misalignments.

### ***Motor Stopper***

The motor stopper is shown in Figure 43.

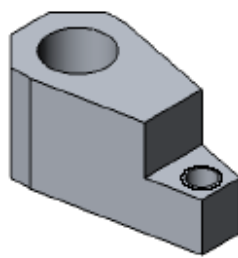


**Figure 43 - Motor stopper**

The motor stopper attaches to the motor shaft using a set screw and creates a moment arm for the stopper bolt. The component was designed to minimize weight. The distance in between the motor shaft and bolt hole was set such that it would have enough clearance to allow rotation of

the stopper around Link 1 without any interference with the motor support. This allows the motor stopper rotate completely around Link 2.

### ***Linear Encoder Support***

The linear encoder support is shown in Figure 44.

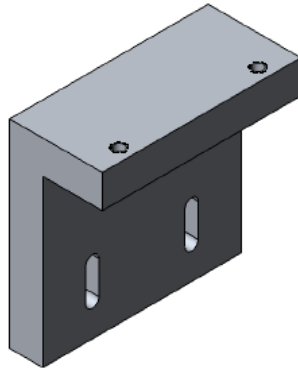


**Figure 44 - Linear encoder support**

The linear encoder support mounts directly onto the mounting plate through the slots shown in the figure. The slots allow the encoder location to be adjusted with respect to the scale mounted onto the rail. This adjustment feature is required to achieve proper a reading from the quadrature encoder and to prevent damage to the linear strip.

### ***Slider Mounting Plate***

The slider mounting plate is shown in Figure 45.

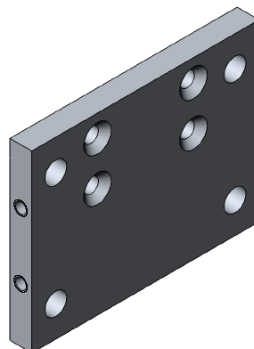


**Figure 45 - Slider mounting plate**

The mounting plate connects Link 3 and the slider of the linear ball bearing to each other. The threaded holes on the side of the plate attach the linear encoder holder next to the linear rail.

## 5.2 Electrical Design

The electrical components for the final prototype were selected to suit the needs of the mechanical design described in Section 5.1 and to fit with the architecture of control system described in Section 5.2.2. Because a rotational-rotational-translational mechanical system was designed, two rotary encoders and one linear encoder were selected to provide position feedback on all links. The control architecture was designed to provide fast response times with a position-controlled brushless DC motor, so a motor, motor controller and microcontroller all had to be specified to suit the project requirements. This section describes the electrical components selected and provides justification for each selection.

### 5.2.1 Encoders

Rotary encoders were selected for Axis 1 and Axis 2, and a linear encoder was selected for the linear ball bearing. Incremental quadrature encoders were designed to fit the software architecture. The primary goal for the rotary encoders was to select the smallest possible encoders with the highest resolution at a reasonable cost. In general, size and resolution are inversely related if cost is held relatively constant so some compromise had to be made to select appropriate encoders. The goal for the linear encoder was to select an encoder that would fit the linear ball bearing with reasonable resolution at minimal cost. Because extremely high resolution significantly increases cost and the design goal was for sub-millimetric accuracy (as opposed to sub-micrometric accuracy), a linear encoder was selected that balanced these needs. Table 5 summarizes the rotary encoder selection process and Figure 46 shows both encoders.

Table 5 - Rotary encoder selection process

Rotary Encoder	Selection Process
Axis 1	<ul style="list-style-type: none"> <li>• Constraint: Physical size &lt; 40 mm</li> <li>• Compromise: The physical size was not a significant limitation so a high resolution encoder was selected. Cost was not a</li> </ul>




	<p>significant factor.</p> <ul style="list-style-type: none"> <li>• Selected encoder: Automation Direct TRDSH-2500-VD</li> <li>• Resolution: 10000 CPR (0.036° resolution)</li> </ul>
Axis 2	<ul style="list-style-type: none"> <li>• Constraint: Physical size &lt; 25 mm</li> <li>• Compromise: The small required physical size of the rotary encoder limited the resolution, but the resolution on Axis 2 was less important than Axis 1 because Axis 2 connected to less linkages. Cost was not a significant factor.</li> <li>• Selected encoder: US Digital S4 Miniature Optical Shaft Encoder</li> <li>• Resolution: 1440 CPR (0.25° resolution)</li> </ul>



**Figure 46 - Axis 1 rotary encoder (left); Axis 2 rotary encoder (right)**

Table 6 summarizes the main alternatives considered for the linear encoder.

**Table 6 - Linear encoder alternatives**

Alternative	Picture	Evaluation
Linear resistive potentiometer		<ul style="list-style-type: none"> <li>• Pros: simple design, enclosed (no contaminants)</li> <li>• Cons: minimum size is too large, very high cost</li> </ul>
Schneeberger linear rail and encoder		<ul style="list-style-type: none"> <li>• Pros: turn-key solution, proven technology</li> <li>• Cons: very high cost (quoted at \$675 + shipping + duty)</li> </ul>
Custom rail and glass scale		<ul style="list-style-type: none"> <li>• Pros: simple design, relatively low cost (linear bearing ~ \$275 + linear encoder and transmissive strip ~ \$75 = \$350)</li> <li>• Cons: custom built mounting</li> </ul>

The custom rail and glass scale alternative was selected because it minimized cost while maintaining a high enough degree of resolution. An NSK linear ball bearing was selected for the mechanical slide, and a US Digital LIN Transmissive Strip with a resolution of 2000 CPI was selected in combination with a US Digital EM1 Transmissive Optical Encoder Module to read the strip.

A resolution analysis was performed with the selected encoders and the mechanical linkage dimensions to ensure that the total expected error due to the encoders was minimal. The error was calculated with the equation below and the results of the analysis are shown in Table 7. The analysis validated the encoder selection because the maximum penetration error due to the encoders was only 0.2 mm and the overall design target was penetration less than 1 mm.

$$\text{Link error} = \text{Link length} * \sin(360/\text{CPR} * \pi/180)$$

**Table 7 - Encoder resolution analysis**

	<b>Encoder 1</b>	<b>Encoder 2</b>
CPR	10000	1440
Degrees per pulse	0.036	0.250
	Link 1	Link 2
Max error (mm)	0.031	0.225
Total Error	0.256	mm

### 5.2.2 Motor and Motor Controller

Motor selection was a major design consideration and one of the most important factors in determining virtual surface rigidity and penetration. Hungr's prototype for two-dimensional haptic surface emulation in a horizontal orientation used a Faulhaber 20 W brushless DC motor connected to a 100:1 gearbox to control the blocker positioning. The requirements for this project were to emulate hard surfaces in three-dimensions in a vertical orientation. As such, the design required a more powerful motor to control both the forces exerted by the surgeon as well as the weight of the robot. After researching various motor and motor controller combinations, the Maxon EC-Max 25W Brushless DC motor (Figure 47) matched with a 66:1 gearbox was selected. It was selected because it provided sufficient nominal torque, acceleration, and maximum velocity for the experimentally derived expected moment of 7.5 Nm (50 N force at 15 cm) discussed in Section 3.



**Figure 47 - Maxon EC-Max motor**

Harmonic drives were considered instead of a gearbox to completely eliminate any backlash from the gearbox but were determined to be too expensive for the project budget (quoted at greater than \$700 for the drive alone). Physical testing of the assembled motor showed that backlash caused negligible errors in the system accuracy. A Maxon EPOS 24/5 motor controller was chosen to complement the motor. The controller was selected because the use of CAN bus as an input increases response time and because the controller has a position control setting that continually updates the motor on its required position. The controller has various preset trajectory generation modes that allow for manual changes to the PID controller gains to adjust system parameters. A 24V – 2.1A power supply was selected for the motor to supply enough power and current to meet the motor's nominal current requirements. In addition, two 4.7nF capacitors are connected in parallel with the power supply to manage peak starting current demand from the motor.

### 5.2.3 Microcontroller

The requirements for the microcontroller were that it had to support CAN communication to interface with the EPOS motor controller, use a high level programming language such as C, and have at least six interrupt ports to support two signals from each quadrature encoder (this is described further in Section 5.3.1). A number of microcontrollers met the requirements with negligible differences in cost; an Atmel AT90CAN128 microcontroller on an Olimex AVR-CAN development board was selected because of the extensive documentation and support available for Atmel microcontrollers. An AVR-JTAG-USB programmer/debugger was also selected to improve programming and troubleshooting.

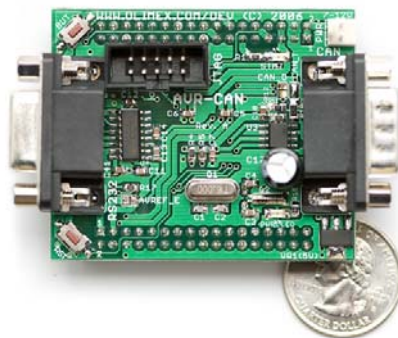


Figure 48 - Development board for Atmel AT90CAN128

### 5.3 Control System Design

The control system was designed to provide significantly faster response times than Hungr's design by using a mechatronics approach. The design is essentially a complete redesign of Hungr's system and eliminates the need for a PC to run the robot. This section describes the control system architecture, user interface and the motor controller design process.

#### 5.3.1 Control System Architecture

Figure 49 shows the architecture of the control system using the electrical components discussed in Section 5.2.

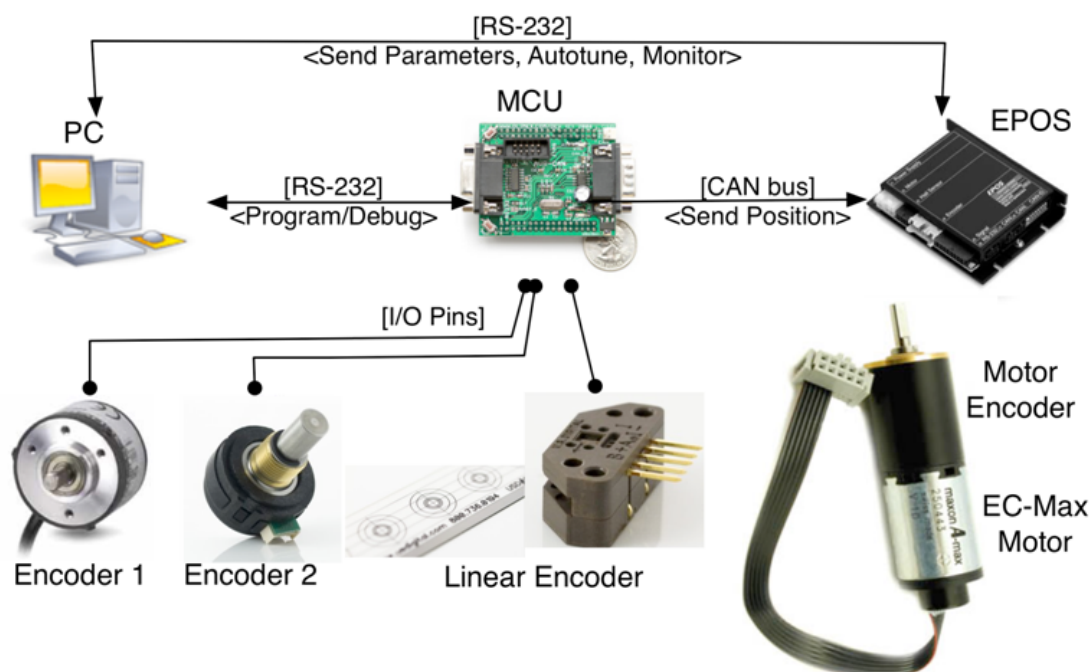


Figure 49 - Control system architecture

Software on the Atmel AVR microcontroller records signals from the three quadrature encoders and calculates position of the end effector in three dimensions. Based on this position, the software algorithm described in Section 5.4 then calculates the required position of the physical blocker. The required blocker position is continually sent from the microcontroller to the Maxon EPOS 24/5 motor controller via CAN communication, and the controller signals the Maxon 25W EC-Max brushless DC motor to move the blocker to its required position. Note that a PC is only



used to program the microcontroller, to tune the PID gains on the motor controller, and to provide feedback on the system response during operation (e.g. motor load graphs). The architecture is a significant improvement over Hungr's system; the use of CAN bus and a dedicated microcontroller yields a much faster response time than the previous arrangement with Hall sensors and a PC. The blocker position is calculated in 706  $\mu\text{s}$  and the communication time between the AVR microcontroller and the EPOS motor controller is 406  $\mu\text{s}$ . Software timing is discussed in further detail in Section 5.4.

The software on the AVR microcontroller was written in C++ and programmed to the AVR's flash memory using a JTAG-to-USB programmer. The AVR runs at 16 MHz and the EPOS controller has a 1 kHz refresh rate, so the response time of the AVR is sufficient for the designed application. At start-up, the microcontroller initializes the CAN bus and sets the EPOS motor controller to the pre-operational state. Constants such as the communication speed, PID gains, software position limits, current limit and operation mode selection are all sent to the EPOS during initialization. This allows the system parameters to be adjusted easily and even during operation using the EPOS user interface to modify the system as necessary for a range of situations.

Each quadrature encoder has two signals (A and B channels) that are wired to separate interrupt ports on the microcontroller – that is, the encoder signals are connected to six separate interrupt ports. The use of dedicated interrupt ports for each encoder signal allows the controller to continuously update the three encoder values at a very high frequency, allowing for high response time and leaving sufficient idle processing time for the remainder of the program.

### **5.3.2 User Interface**

The user interface, shown in Figure 50, is comprised of five buttons and three status LEDs that are all wired to separate input/output ports on the AVR microcontroller. There is a green start button used for initializing and calibrating the system, a large red emergency stop button for disengaging the motor and resetting the controller, and three small red profile selection buttons that also function as the status LEDs. The system has automatic fault detection: any faults from

the motor controller are detected by the AVR and can be cleared once the problem is fixed. A description of how to use the system is provided below.

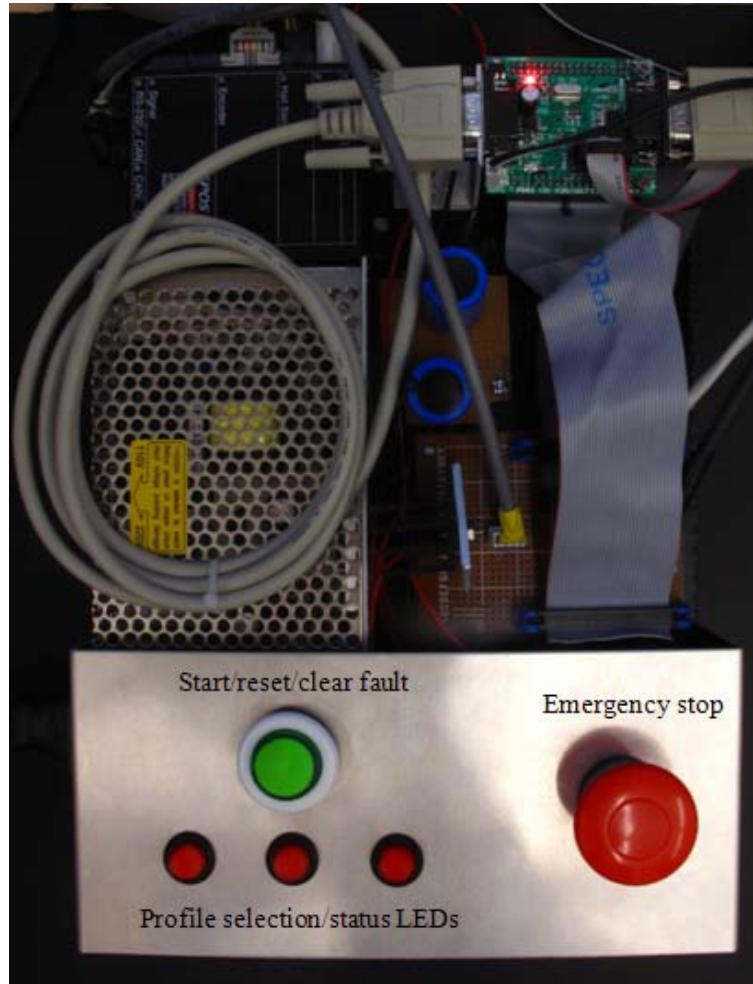


**Figure 50 - User interface and control board**

The system must be setup correctly in order to operate as expected. The motor must be as far counter-clockwise (when viewed from the top) as possible before the power supply is plugged in. Once the motor is correctly positioned and the power supply is connected, the three status LEDs blink twice to indicate there is power. The robot must then be put in the “home” position, shown in Figure 51, in order for the encoder positions to properly initialize. While in this position, the user presses the green start button and the LEDs slowly light up as the system initializes.

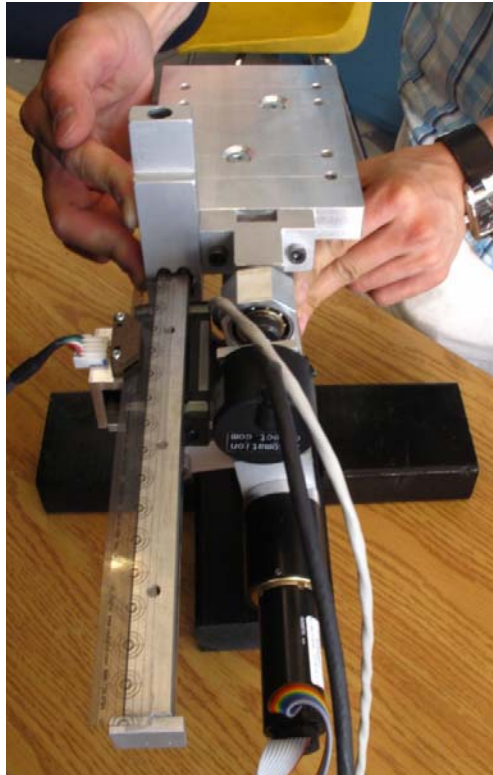


**Figure 51 - "Home" position**

Once the system is ready, the LEDs blink in quick succession to inform the user that it is ready for a shape to be selected. The user then presses one of the three buttons to choose a shape. Once pressed, the motor engages to emulate the virtual hard surface selected and the system is functional.

If at any point a fault is detected, the LEDs all blink very quickly at the same time. A fault could be triggered if the motor cables are disconnected or if the software has sent an erroneous position signal. In order to clear the fault, the user simply has to press the green start button and reselect a shape.

### 5.3.3 Controller Design

The Maxon EPOS 24/5 motor controller selected is a PID controller. The block diagram for the controller is shown in Figure 52 (courtesy of Maxon Motor Control).

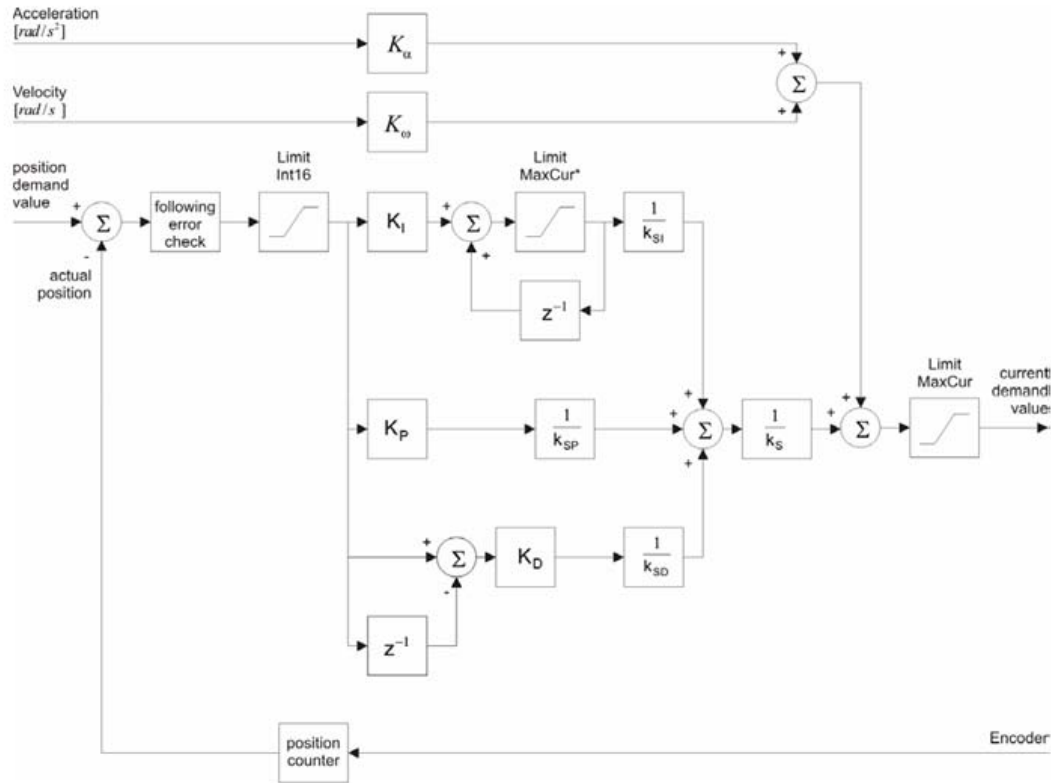


Figure 52 - EPOS 24/5 block diagram (photo courtesy of Maxon Motor Control)

The constants for the fixed parameters defined by Maxon are listed in Table 8.

Table 8 - Fixed controller parameters

Constant	Value
$k_{SP}$	8
$k_{SI}$	64
$k_{SD}$	1
$k_S$	2

The 'Position Demand Value' setting was selected to update the motor with the desired blocker position during operation. As such, the PID gains  $K_P$ ,  $K_I$ , and  $K_D$  had to be optimized to produce smooth virtual profiles with sufficient rigidity. A load test was designed to perform a frequency sweep at the expected load to determine the crossover frequency of the plant (the user's hand).

The test was performed by rigidly attaching a mass to a lever connected to the motor and varying the frequency as the motor oscillated back and forth.

The results of the load test, shown in Figure 53 and Figure 54, showed that instability occurred past 20 Hz, but the results were mostly inconclusive. The experimental setup itself was not ideal – simulating a user pushing an end effector against a virtual surface proved difficult to perform. As such, a different approach was taken to design the PID gains.

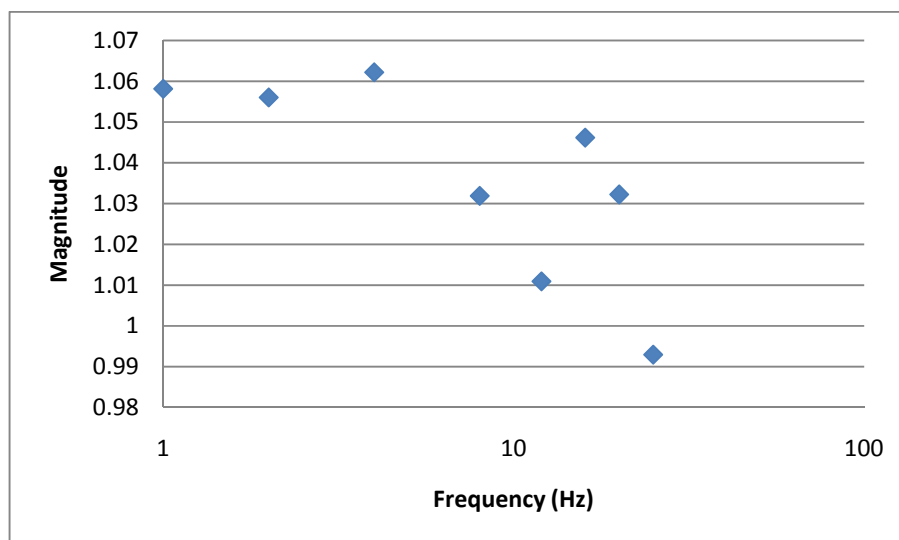


Figure 53 - Magnitude vs. frequency for load test

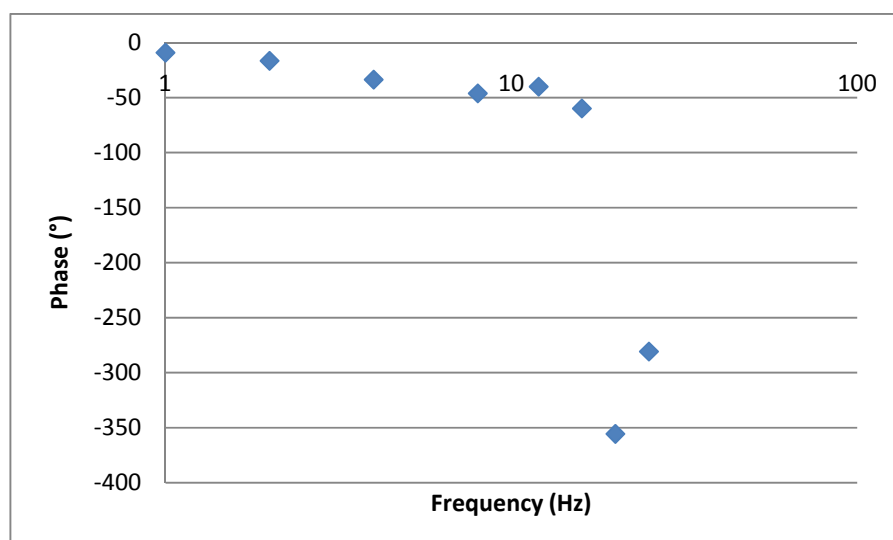
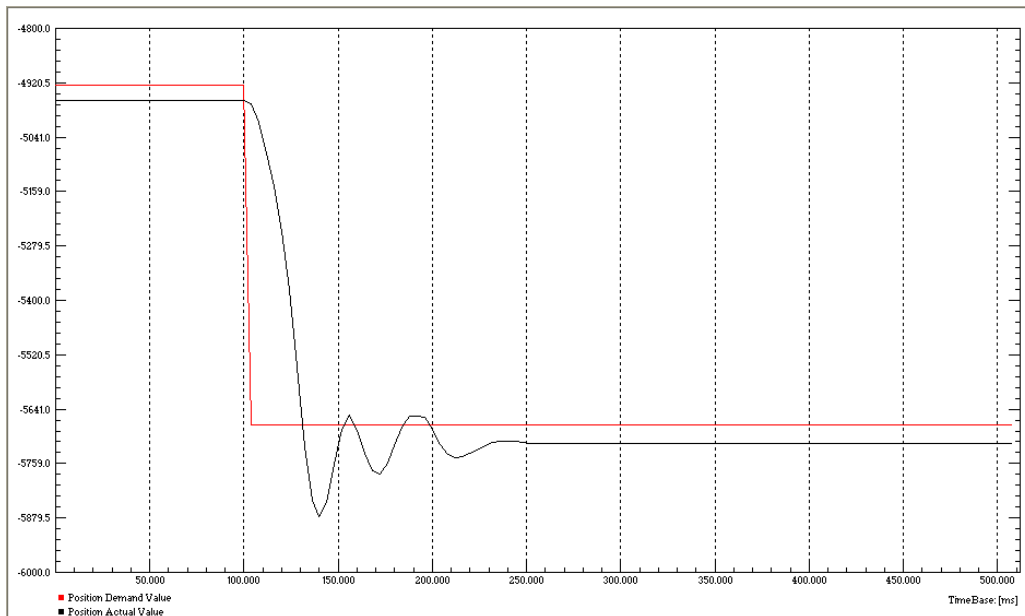
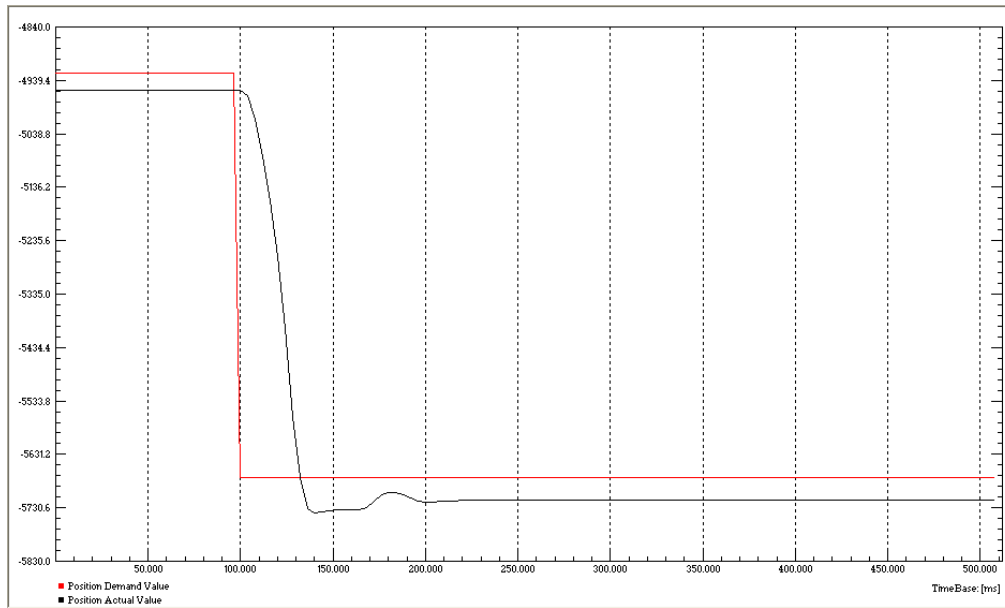


Figure 54 - Phase vs. frequency for load test

Because the load test was inconclusive, a different approach was taken to optimize the PID gains. The EPOS user interface was used to select values for  $K_P$ ,  $K_I$ , and  $K_D$  iteratively and with certain performance characteristics in mind. The target for the controller was to provide a fast response time with minimal surface penetration. The proportional gain,  $K_P$ , was increased to provide a faster response time at the cost of instability and oscillation. The integral gain,  $K_I$ , was increased to eliminate steady-state error at the cost of larger overshoot. The derivative gain,  $K_D$ , was increased to eliminate overshoot at the cost of transient response time. Figure 55, Figure 56, and Figure 57 show a representative sample of the iterative process used for step responses of a user hitting the end effector against the virtual surface at normal load. Overshoot is reduced between Figure 55 and Figure 56 by increasing  $K_D$  and steady-state error is reduced between Figure 56 and Figure 57 by increasing  $K_I$  while varying the other two parameters as necessary. The final values selected for users tests are those in Figure 57:  $K_P = 100$ ,  $K_I = 10$ ,  $K_D = 200$ .



**Figure 55 - Step response ( $K_P = 64$ ,  $K_I = 0$ ,  $K_D = 20$ )**



**Figure 56 - Step response ( $K_P = 64$ ,  $K_I = 0$ ,  $K_D = 50$ )**

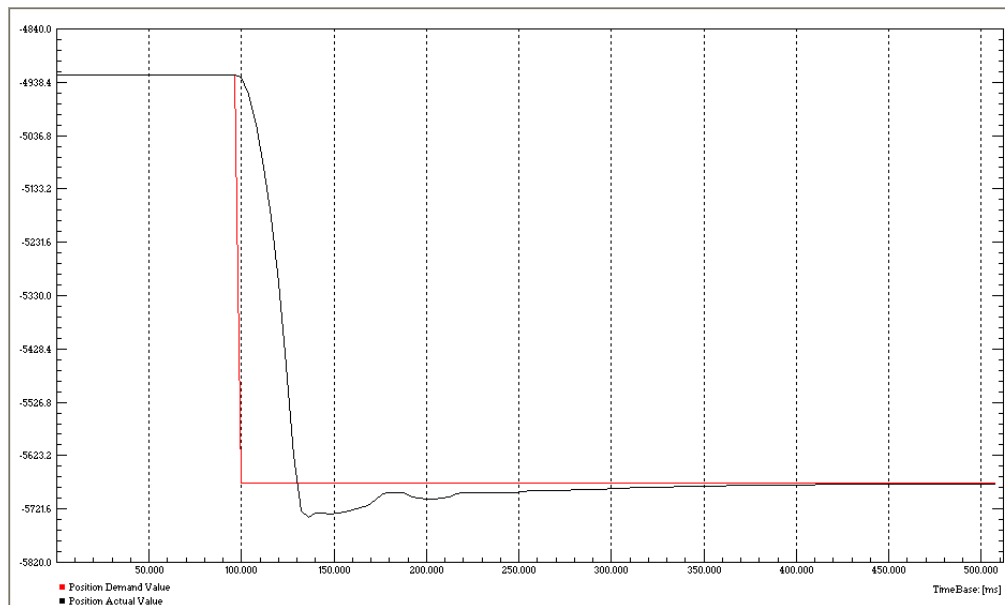


**Figure 57 - Step response ( $K_P = 100$ ,  $K_I = 10$ ,  $K_D = 200$ )**

User tests reported that the virtual surface was very rigid and the profiles were adequately designed, but the motor response was slightly “jerky” at steep inclinations because the motor responded too quickly. Further testing and optimization of the PID gains would mitigate this problem; proposed future work is discussed in detail in Section 7.

## 5.4 Algorithm Design

Hungr noted problems with lateral deflection and hysteresis in his design due to low sensitivity in regions where the end effector was extended further. A drawing of Hungr's linkages is shown in Figure 58. His design only had one encoder at the base of Link 1 ( $\theta_1$ ) which was used to calculate the dynamic blocker position using an inverse kinematics algorithm. As a result, his prototype performed poorly when drawing flat horizontal lines, particularly in the extreme side regions. In extended regions, relatively small changes in the angle at the base led to large angle changes between Link 1 and Link 2 ( $\theta_c$ ). Since the dynamic hard constraint worked by limiting the angle between Link 1 and Link 2, operation in extended regions led to low sensitivity in the control of the motor.

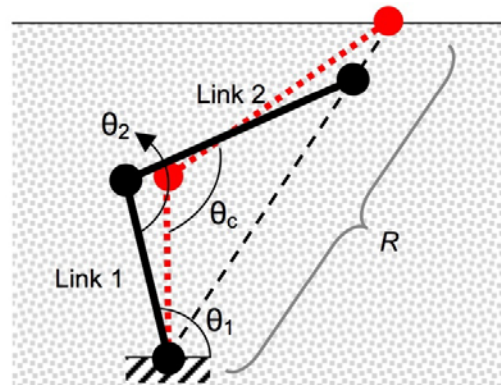
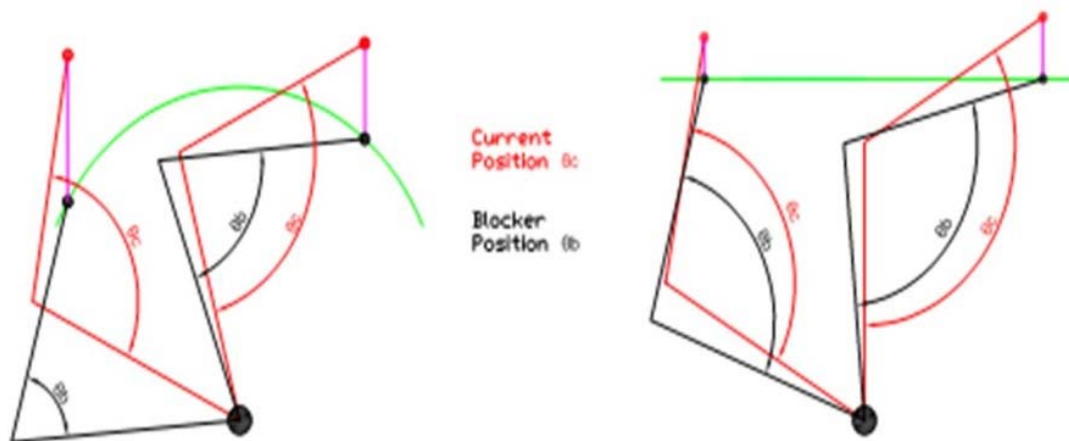


Figure 58 - Hungr's linkage orientation

The three-dimensional haptic design presented here uses a forward kinematics algorithm to reduce instability in extreme regions. By placing a second rotary encoder on Axis 2, the current X-Y position of the end effector ( $\theta_c$ ) is determined. This information is used to measure how far the current end effector position is from the testing profile in the Y-direction. This is used to predict where the motor blocker ( $\theta_b$ ) should be positioned in order to block the end effector from penetrating the virtual surface should it move straight down in the Y-direction. The blocker X-Y position is calculated by using the same X-coordinate as the current end effector position and then calculating the Y-coordinate of the virtual surface at that X-position.  $\theta_b$  is calculated using the cosine law using the length of Link 1, Link 2, and the radial distance from the blocker X-Y position to the base Axis 1. Figure 59 illustrates the algorithm.





**Figure 59 - Blocker position algorithm**

A linear encoder is used to extrapolate the algorithm into three-dimensional space. The algorithm calculates the current end effector position along the Z-axis. Defining a three-dimensional surface profile can be thought of as defining X-Y contours along the length of the Z-axis. The two rotational linkages control movement in the X-Y plane and the X-Y surface profiles are updated as the Z-axis position changes.

Optimizing the algorithm to reduce computational time was a major consideration for the design of the controls system. Two different options were evaluated to define virtual surfaces. The first option evaluated was a three-variable lookup table, in which a matrix of X-Y-Z points forms a three-dimensional surface profile. The current X- and Z-positions of the end effector are used to lookup the corresponding Y-positions for the surface profile. A binary searching algorithm is employed to search the lookup table to find the closest values that match the current X- and Z-positions. Linear interpolation is then used to determine the corresponding Y-position. Having a larger lookup table would increase the resolution between points for the defined surface profiles, but would also require more iteration to search through the larger matrix and increase computational time. The linear interpolation calculation would also increase computational time. This option was not pursued due to our limits of the microcontroller; the microcontroller only had 128 Kb of flash memory storage, which restricted the lookup table size to be a 40x40x40 matrix of float numbers. Given the high precision of the quadrature encoders selected, using a lookup table with such low resolution would be a bottleneck for performance. However, if the microcontroller had sufficient memory to store a large lookup table, this method would be

advantageous for complex geometric profiles that can not be easily calculated by simple equations.

The other alternative was to perform real-time computations for the surface profiles – this alternative was chosen for the project. For testing purposes, only simple profiles such as ellipsoids, flat planes and sine waves were evaluated. This allowed simple real-time calculations to be performed whenever the position of the end effector changed. Testing determined that for simple profiles it was faster to compute in real-time than it was to use lookup tables. Sine and cosine lookup tables were also considered to speed up computational times, but were determined to be slower than computing trigonometric functions using the built in Taylor series approximations in the C programming language. Performing real time calculations for surface profiles takes approximately 11,300 clock cycles and communication time takes 6,500 clock cycles. The selected microcontroller runs at 16 MHz, so the computational and communication operations take 706  $\mu$ s and 406  $\mu$ s, respectively. The Maxon EPOS 24/5 motor controller used samples at 1 kHz frequency (1 ms period) clock cycles, so the computational and communication times take slightly longer than the motor controller sampling times. Further optimization on the algorithm, communication, and motor controller response times are possible and are described in Section 7. However, given the success of the two- and three-dimensional test results presented in Section 0, the controls design successfully met the requirements of our design.

## 6. Testing and Results

Several tests were designed to test the performance of the final prototype. Various surface profiles were defined to test different aspects of the prototype design and geometric profiles defined by simple equations were used. Both the two- and three-dimensional surface profiles were based on three simple shapes: ellipse, sine bump, and straight line. The test profiles used were similar to those that Hungr used in his research. The ellipse profile tested the prototype's ability to follow smooth curves, whereas the flat line tested a wide range of motion for the blocker. The most difficult test profile was the sine bump, which tested the prototype's ability to trace small features that required large, sudden changes in the blocker position. The mechanical design limited the angle between Link 1 and Link 2 to rotation below  $60^\circ$ . This meant that the prototype could not access any region within a 50 mm radius of the base mount. As a result, all test profiles were defined within the accessible region shown in Figure 60. The results from two-dimensional tests in the X-Y and Y-Z planes are presented in this section along with the results from three-dimensional tests.

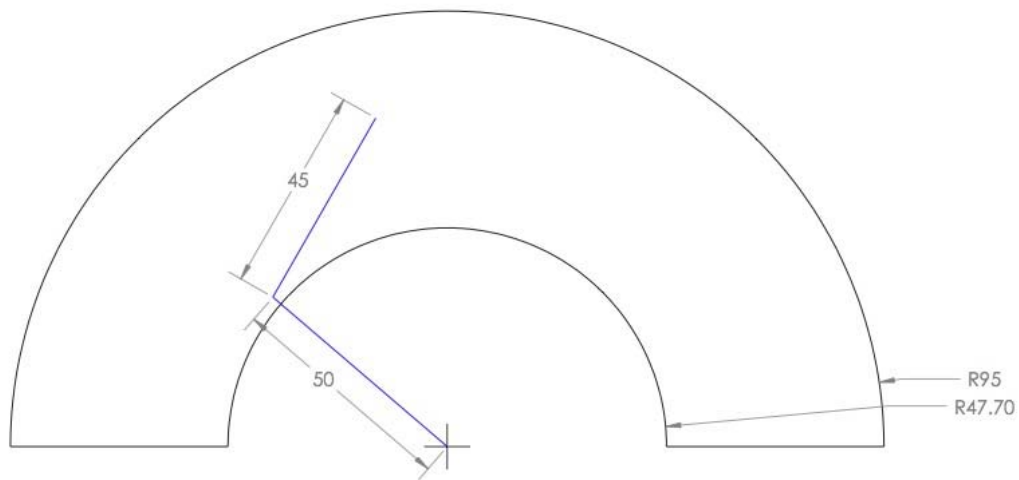
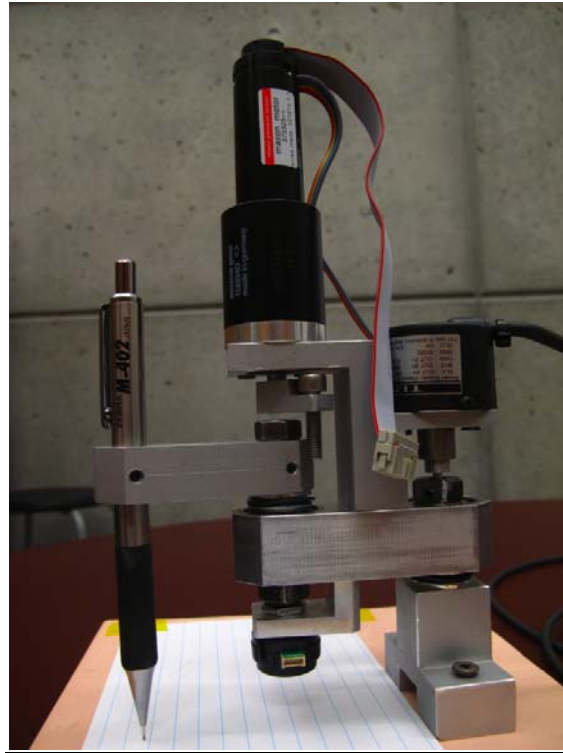


Figure 60 - Accessible regions of prototype

### 6.1 X-Y Plane 2-D Test Results

Similar to Hungr's testing procedures, two-dimensional profile pen tests were conducted in the X-Y plane to test the performance of the two rotational linkages. Figure 61 shows the setup of

the prototype for the X-Y plane tests. To perform these tests, the linear slider components were detached and a pen was fit through the hole at the end of Link 2.



**Figure 61 - X-Y plane setup**

The straight line was the first profile tested – the results are shown in Figure 62. Drawing a straight horizontal line using the two rotational linkages required large angular displacements on both Axis 1 and Axis 2, which meant that the blocker underwent a wide range of motion to complete the line. Hungr's design encountered the greatest difficulty with this profile.

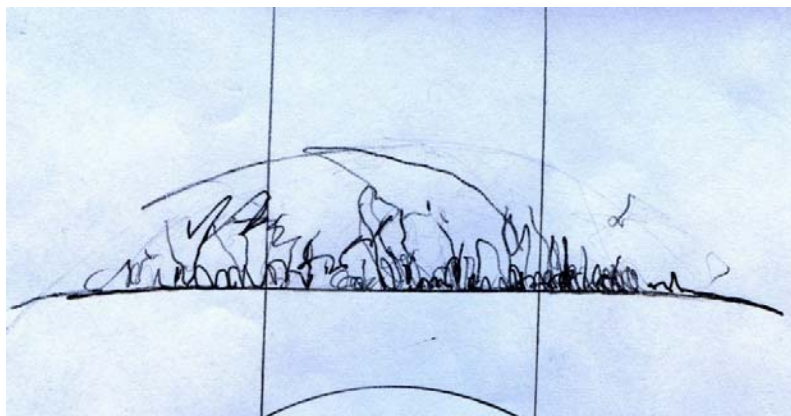


**Figure 62 - X-Y plane 2-D test: straight line**

The prototype performed exceptionally well on the straight-line test, as there were no penetrations through the surface boundary. The slightly rounded edges on the extreme left and right regions are due to the limitations of the rotational linkages when fully extended. Hungr's prototype encountered problems with hysteresis in these regions mainly because of the inverse kinematics algorithm used to control the blocker. As described in Section 5.4, hysteresis errors are greatly reduced by the forward kinematics algorithm used in the design presented in this report.

The ellipse profile was tested next – the results are shown in Figure 63. This profile was expected to be the easiest test for the prototype because gradual curved profiles closely follow to the natural movement of the rotating linkages. The blocker effectively constrained the pen from penetrating the defined boundaries, even as significant amounts of force were applied against the surface boundaries. No hysteresis error was observed during the ellipse test.



**Figure 63 - X-Y plane 2-D test: ellipse**

The third profile that was tested was the sine bump, which consisted of a horizontal line with a sharp sine curve in the middle as shown in Figure 64. This was expected to be the most challenging test since it required sudden changes in the blocker position as it approached the sine curve. There were some small hysteresis errors observed on the left side of the sine bump, but the right side of the sine bump was much more accurate. The geometry of the rotating linkages appeared to push the user quickly down the bump when the end effector was operating on the left side of the sine bump because the blocker applied a force in a direction similar to the profile. Small errors may have resulted because the blocker response time may not have been fast enough to respond to the quick movements. On the right side of the sine bump, the blocker

applied a force perpendicular to the surface profile so it resisted penetration of the boundary more readily.

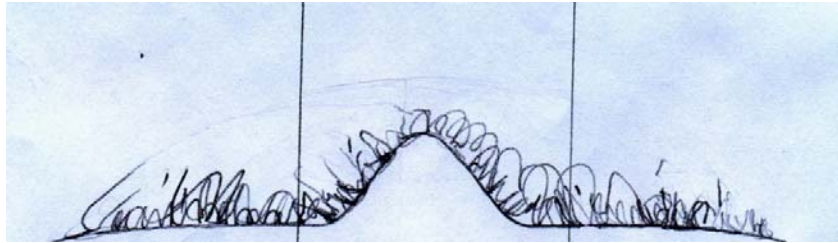


Figure 64 - X-Y plane 2-D test: sine bump

## 6.2 Y-Z Plane 2-D Test Results

Pen tests were conducted in the Y-Z plane in addition to the two-dimensional tests in the X-Y plane. The setup for the Y-Z plane tests is shown in Figure 65. This setup tested the accuracy of the prototype using the rotating linkages and the linear slider. This test demonstrated the performance of the prototype in three-dimensions because it required all three encoder inputs to compute the blocker position.

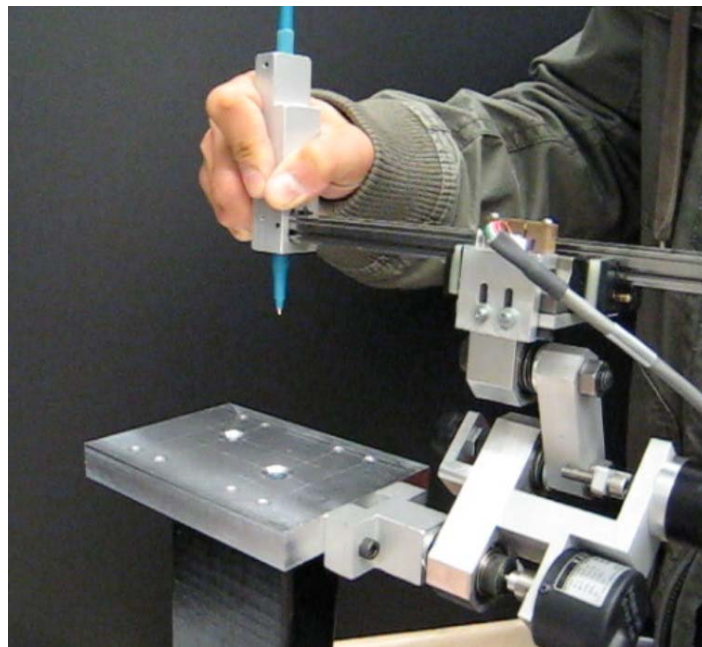
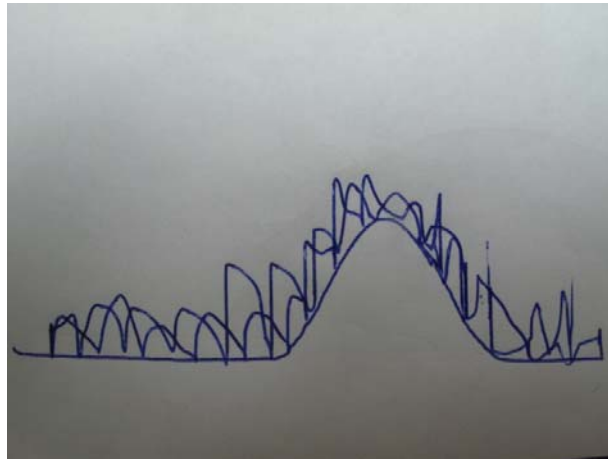


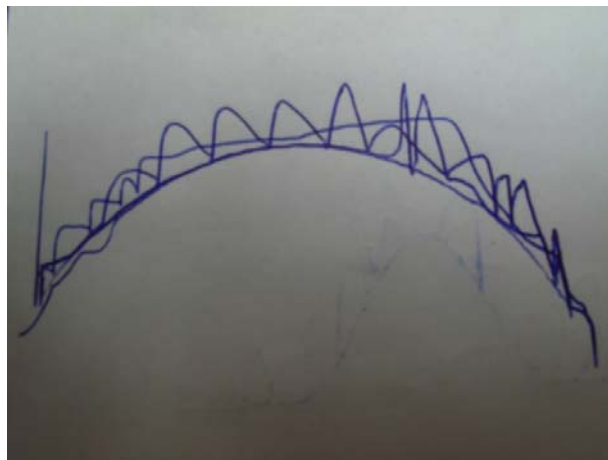
Figure 65 - Y-Z plane test setup



Figure 66 shows the results of the sine bump test and Figure 67 shows the results of the ellipse test in the Y-Z plane. There were slight surface penetrations in both of these tests, but the errors may have been due to the use of non-rigid plastic pen (a stiff metal pen was unavailable so a deformable plastic pen had to be used). Overall, the Y-Z tests performed exceptionally well: minimal hysteresis error was observed and the results were comparable to the X-Y plane tests.



**Figure 66 - Y-Z plane 2-D test: sine bump**



**Figure 67 - Y-Z plane 2-D test: ellipse**

### **6.3 3-D Milling Tests**

After conducting pen tests in two-dimensions, a milling tool was installed in place of a pen as the end effector to conduct tests in three-dimensions. Before actually using the milling tool to carve out three-dimensional shapes on a block of wood, the prototype's ability to restrict motion in free

space was tested. Although the accuracy of the prototype for this test was not quantitatively measured by these tests, it was useful to determine the feel of system as it was operated in three-dimensional space. Figure 68 shows the setup for these tests. The motor supplied sufficient torque to restrict penetration into the defined surfaces in the vertical orientation, where the motor blocker had to counter both the weight of the system prototype as well as the applied forces from the user.

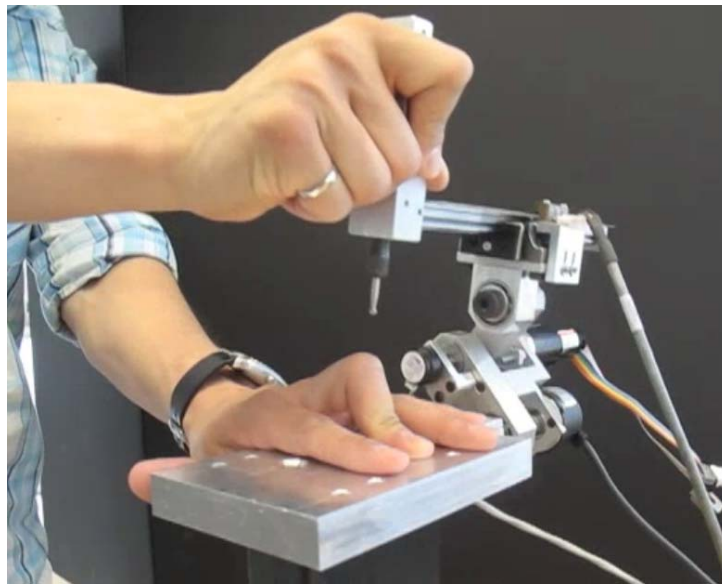


**Figure 68 - 3-D free space test setup**

The three-dimensional surface profiles that were tested are similar to those used for the 2D tests. They included a flat plane, sine bump, and ellipsoid as shown in Figure 69, Figure 70, and Figure 71, respectively. The prototype performed very well during these tests. Movement along the surface boundaries was smooth and motion was unrestricted when the end effector was not in contact with the surface boundaries. The blocker was able to withstand impact forces against the virtual surface without observable penetration. Multiple users tested the robot in free space operation and were asked to comment on their experience. All users responded that the virtual surface profiles were readily apparent to them and that the blocker provided a realistic hard constraint against penetration of the surface.



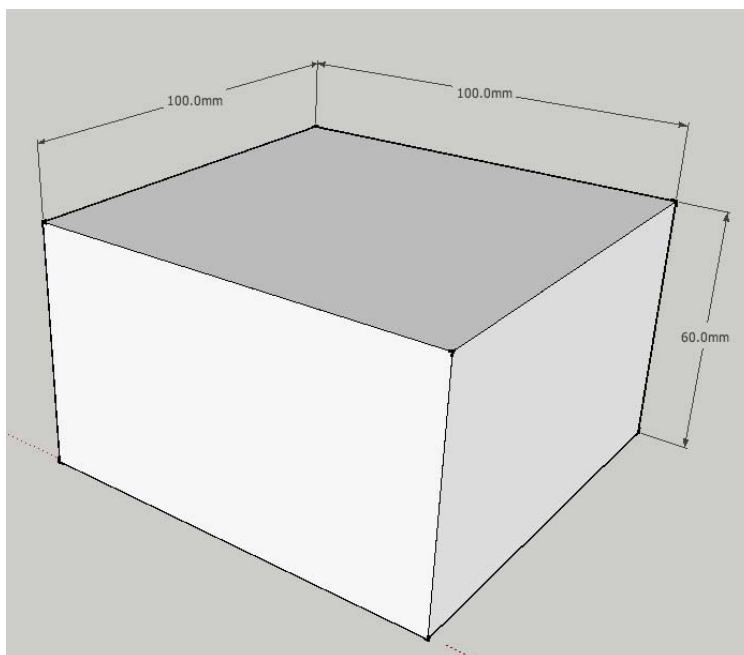


**Figure 69 - 3-D test profiles: flat plane**

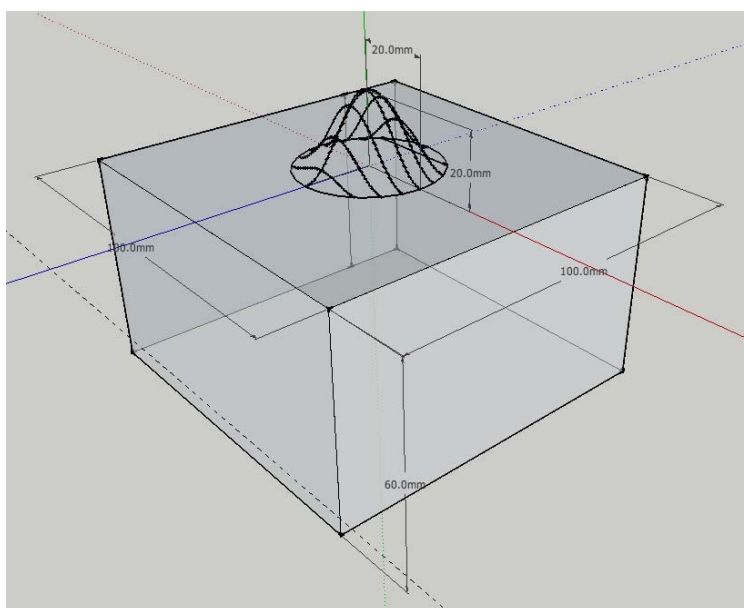


**Figure 70 - 3-D test profiles: sine bump**

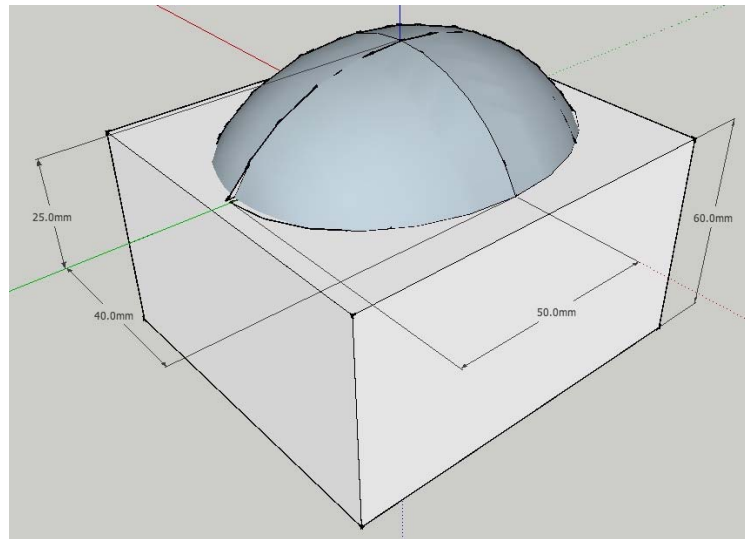


**Figure 71 - 3-D test profiles: ellipsoid**

The final test for the prototype was to use a milling tool to carve out three-dimensional profiles out of blocks of chemical wood. A spherical milling bit was connected to a Dremel motor using a flexible shaft used to act as the end effector. In order to protect the exposed bearings on the mechanical components from debris, a plastic bag was wrapped around the entire robot with a small hole cut out for the milling tool. The setup used for the milling test is shown in Figure 72.



**Figure 72 - 3-D milling test setup**

The prototype successfully carved out the defined surface profiles on blocks of chemical wood, but the size of the spherical milling bit used was too small to remove enough material to fully carve out the defined three-dimensional shapes. Instead, only small lines were carved out to determine if the milling tool produced the desired profiles in certain sections. For the sine bump test, a single vertical and horizontal line was carved out through the middle of the block and was observed to match the defined dimensions of the profile. Quantitative results on the accuracy of the prototype in the full three-dimensional range of motion can be obtained in future tests with a larger milling bit and a higher power Dremel motor remove material more efficiently.

## **7. Future Work**

The prototype designed successfully met the majority of the project requirements, but is only a proof-of-concept prototype that has laid the foundation for future work. Significant work is required to produce a commercially viable product for use in actual surgery. This section presents suggested future work for the mechanical and electrical/controls systems.

### **7.1 Future Mechanical Work**

There are a number of mechanical design changes that would improve the system performance. Each change is briefly discussed here.

#### ***Overall Size Reduction***

The critical dimensions of the final designed prototype were based in part on analysis and calculations performed by Hungr (2008). All other dimensions were selected in a conservative manner in order to minimize or eliminate possible deflection due to extreme applied loads during operation. Performing further finite element analysis tests and linkage optimization could potentially help to reduce the size of the entire device. A reduction in size would help reduce the weight, which would improve the system response and reduce the required motor torque.

#### ***Bearings: Size Reduction and Sealing***

The prototype designed uses general purpose, non-precision, open ball bearings with 15° contact angles (Figure 73). This type of bearing is suitable for applications that are specifically designed to meet tight ABEC standards and handle typical radial loads. The testing phase illustrated that dust and external debris could be detrimental to bearing performance if the bearings are not sealed. One possible solution is to replace the open ball bearings with double sealed bearings which block out contaminants and preserve lubricants. Another solution would be to use ultra-thin, multi-load bearings sealed in a casing which could be sterilized if necessary. For sterilization purposes, it would be better to use stainless steel bearings instead of regular steel bearings. Stainless steel bearings provide the same strength as steel bearings but offer superior

corrosion resistance. A potential third solution is to use Delrin ball bearings. These types of bearings are significantly lighter in comparison to steel bearings, perform smoother, are quieter and are corrosion resistant.

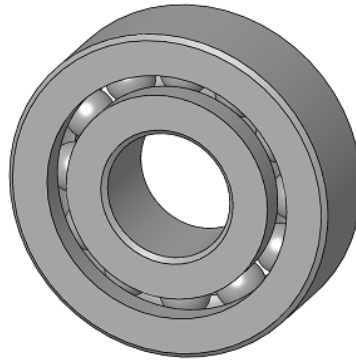


**Figure 73 - General purpose, open ball bearing**

### ***Linear Slide Bearing Design Changes***

The size, mass and material of the linear slider bearing used in the design (Figure 74) can be improved. With a mass of over 0.5 kg, the linear ball bearing and railing account for more than 40% of the prototype's weight. Using a less dense material than hardened steel could help reduce the weight. Another change would be to eliminate the counter bored holes used for the rail to be secured on any surface and for the greasing unit to move back and forth along the shaft. These holes pick up debris and chipped material and can hinder the slide's performance.

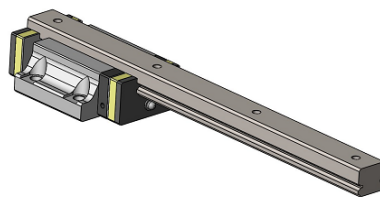


**Figure 74 - Linear ball bearing with sliding rail**

The linear encoder used in the design came with a separate transmissive strip that required a custom built stand, as shown in Figure 75. The reader is prone to contamination from grease and debris in the current design. It would be ideal if the encoder could have a built-in linear strip or a seal for the encoder. The encoder location could also be optimized to provide the greatest range for angle of attack.

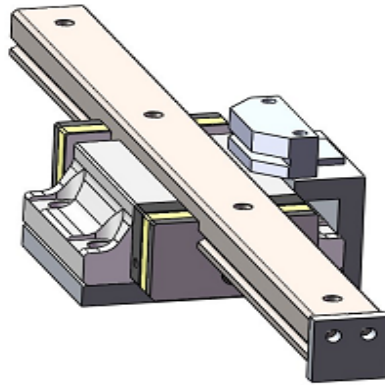


**Figure 75 - Linear encoder with stand**

### ***Link 3 Dimension Optimization***

The dimensions of Link 3 (Figure 76) can be optimized. The distance between the centre of the bearing's casing and the top surface of the platform is currently 25 mm. This is a critical length because it determines the range of the end effectors extension. Optimizing this length may lead to a greater range of motion and a wider range of attack angle. Another design change that could help is to make the link extendable so that it can be extended or retracted for a variety of circumstances.

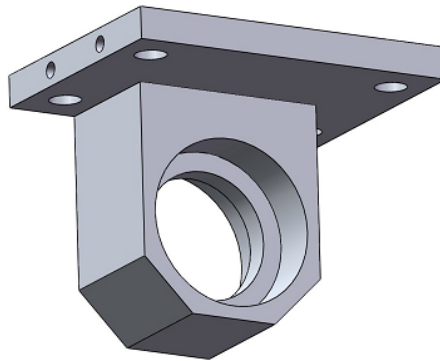


**Figure 76 - Link 3**

### ***Replace the Motor Set-Screw with a D-Hole***

Avoiding set screws is ideal for any design, especially to transmit torque. Due to continually changing design requirements and time and material constraints, a set-screw mechanism was used to keep the blocker fixed to the motor's shaft, as shown in Figure 77. Use a D-hole punch

instead of a set screw would be one method of eliminating the set screw to fix the blocker to the motor shaft.

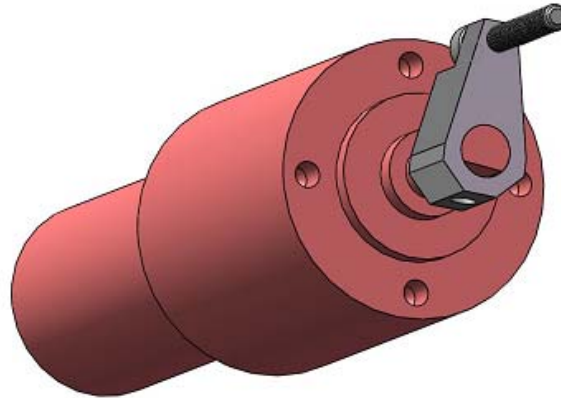


Figure 77 - Motor and motor blocker

### ***Motor Stopper Material***

Throughout the testing phase and later stages of the project, it was evident that Link 2 was wearing out in the position of contact with the blocker. This occurred because a stainless steel screw was used as the physical stopper mechanism, whereas the link was made out of aluminum (Figure 78). One way to resolve this issue is to file down or lathe the threads on the screw. Another possible solution is to thread the end of an aluminum rod and use it as the blocker in place of the stainless steel screw.

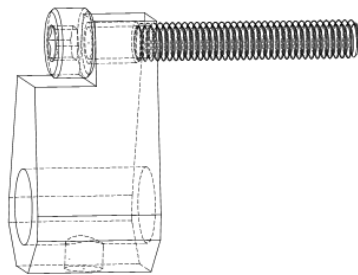


Figure 78 - Motor stopper and screw

### ***Machined Shafts instead of Shoulder Screws***

Modified shoulder screws were used for Axis 1 and Axis 2 as illustrated in Figure 79. It would be ideal if the links were machined shafts instead of shoulder screws to improve the tolerance

between the links and the two axes. Customizing the axes by machining would also enable the dimensions to be altered, which could reduce the weight of the device.

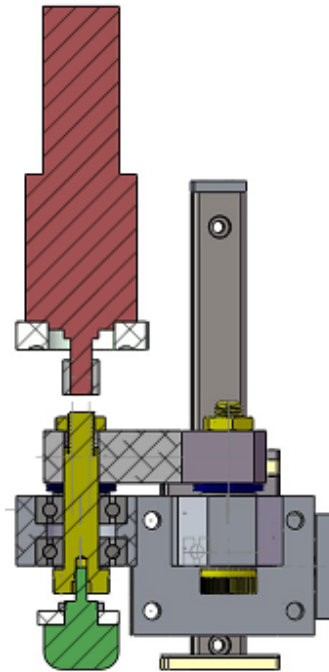


Figure 79 - Section view of the shoulder screws used for Axis 1 and 2

### ***Larger Milling Bit***

Although a cutting device was not actually within the scope of the project, a milling tool was incorporated into the design. The 3.0 mm spherical milling bit, shown in Figure 80, was used as an end effector during the testing phase. It was immediately apparent that the milling bit was too small for the application; a larger milling bit would improve surface finish (less scallop lines) and reduce milling time. According to discussions with Plaskos and Hodgson, typical surgical milling bits are between 3 mm and 20 mm, so using a larger milling tool would be a logical step.



Figure 80 - Spherical milling bit



### ***Sterile Components***

A commercial surgical robot would eventually be required to be sterilized before operation. Components selected for the design such as the encoders and the motor would not be able to withstand the autoclave environment required for sterilization. A possible solution for these components is to seal them in a casing that can withstand the sterilization process.

### ***Flexible Coupling***

Due to extremely tight tolerances and minor machining errors there was some small resistance in the movement of the linkages. This issue was especially evident at the connection between Encoder 1 and Axis 1, as shown in Figure 81. The best solution to this issue is the use of plastic couplings that could prevent components from becoming over-constrained; this would also increase the durability of the design.

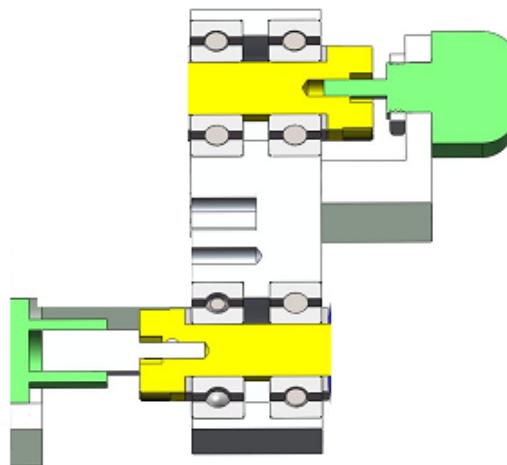


**Figure 81 - Encoder connections with flexible couplings**

### ***Range of Motion***

The final prototype design allows for a 120° range of motion. This could be improved with reduced dimensions. Improving the range of motion for the device would be ideal because the design objective is to cover maximum volume for a device of given size.

## **7.2 Future Electrical and Controls Work**

To improve the overall design, several changes could be made to the electrical components and control system design. Each change is briefly discussed here.

### ***Motor and Gearbox Weight***

The motor and gearbox in the current design are very heavy and make the ergonomics of the system somewhat uncomfortable. To reduce this weight, a different motor could be used. For example, a stepper motor would reduce the need for the large gear ratio, which contributed greatly to the overall weight.

### ***Quadrature Encoder Index Lines***

The encoders used were incremental quadrature encoders without index lines (the linear encoder had an index line but it was not used). Using absolute encoders would eliminate the need for initial calibration when the robot starts up and would make the device more user friendly.

### ***Cable Stiffness***

The encoders and motor all have large cables that have noticeable stiffness when the robot is moved. These cables could be better fastened and supported or custom wiring could be created to reduce the large number of bulky cables.

### ***Motor Controller and PID Gains***

The motor controller has a maximum refresh rate of 1 kHz. If this controller speed is insufficient, a faster PID controller can be used. The gains of the PID controller can be adjusted to better simulate a hard constraint and reduce jittering that occurs with certain features. In particular, the proportional and derivative gains can be reduced to allow the system a small amount of overshoot – this could help eliminate jitter.

### ***Flipped Linkage Algorithm***

The current system only operates when the linkages are flipped in a certain orientation. By adding code allowing for flipped linkages to the blocker position algorithm, the robot could still operate when the linkages are flipped in the opposite orientation.

### ***Complex Shapes***

Currently, the only shapes that can be milled are expressed geometrically and have to be programmed into the microcontroller manually. With more flash memory, the shapes could be instead expressed using point clouds with a look-up table which the algorithm would access. The shapes could then be created with a laser scanner or three-dimensional CAD software and uploaded directly to flash memory for the controller to use.

## **8. Conclusion**

This report provided a comprehensive analysis of the design process involved in creating a prototype capable of emulating three-dimensional virtual surfaces using haptic technology. Existing commercial technologies and research were explored to identify functional requirements for the design, basic and detailed concepts were developed and examined to meet the functional requirements, the final design and its individual components were presented in detail, testing results and their significance were explored, and recommendations for future work were provided.

A mechatronics approach involving integration of mechanical and electrical components with a controls system and software algorithm was used to develop the prototype. The prototype was developed according to specific design objectives related to virtual surface emulation.

Overall, the developed prototype was a success. The prototype met the functional requirements and was well received by users. It was able to emulate rigid virtual surfaces in two- and three-dimensions. The test results suggested that haptic emulation technology has the potential to become commercially viable with further development. Suggestions for future work were provided, particularly for the mechanical and electrical/controls systems.

Based on the findings of this report, future development of haptic emulation technology for three-dimensions is recommended. The design presented in this report is an effective proof-of-concept prototype, but further work is necessary to refine and optimize the technology for surgical applications. With further development, haptic emulation has significant potential to improve surgery for patients and surgeons alike.

## 9. References

Book, W, R Charles, H Davis, and M Gomes. "The Concept and Implementation of a Passive Trajectory Enhancing Robot." *Proceedings of the ASME International Mechanical Engineering Conference and Exhibition*. 1996. 58:633-638.

Brisson, G, T Kanade, A DiGioia, and B Jaramaz. "Precision Freehand Sculpting of Bone." *Proceedings of MICCAI 2004*. 2004. 105-112.

Colgate, J E, W Wannasuphoprasit, and M A Peshkin. "Cobots: Robots for Collaboration with Human Operators." *Proceedings of the International Mechanical Engineering Congress & Exposition (IMECE)*. 1996. 58: 433-439.

Harris, S J, B Davies, and M Jakopc. United Sates of America Patent 2004/1028026 A1. 2004.

Hayward, V, and K E MacLean. "Do It Yourself Haptics, Part I." *IEEE Robotics and Automation Magazine*, 2007.

Ho, S C, R D Hibberd, and B L Davies. "Robot Assisted Knee Surgery: Establishing a Force Control Strategy Incorporating Active Motion Constraint." *IEEE Engineering in Medicine and Biology*, May/June 1995: 14(3):292-300.

Hungr, Nikolai Anthony. "Haptic Emulation of Hard Surfaces with Applications to Orthopaedic Surgery." Vancouver, British Columbia: University of British Columbia, 2008.

Kuchenbecker, K J, J Fiene, and G Niemeyer. "Improving Contact Realism Through Event-Based Haptic Feedback." *IEEE Transactions on Visualization and Computer Graphics*, March 2006: 12(2):219-229.

Lawrence, D A, and Chapel J D. "Performance Tradeoffs for Hand Controller Design." *Proceedings of the 1994 IEEE International Conference on Robotics and Automation*. 1994. 4:3211-3216.

Lawrence, D A, and J D Chapel. "Performance Tradeoffs for Hand Controller Design." *Proceedings of the 1994 IEEE International Conference on Robotics and Automation*. 1994. 4:3211-3216.

Peshkin, M A, J E Colgate, and C Moore. "Passive Robots and Haptics Displays Based on Nonholonomic Elements." *Proceedings of the 1996 IEEE International Conference on Robotics and Automation*. 1996. 551-556.

Roche, M. "Changing the Way Surgeons Plan and Execute Minimally Invasive Unicompartamental Knee Surgery." *Orthopaedic Product News*, July/August 2006.

Salisbury, K, D Brock, T Massie, N Swarup, and Zilles C. "Haptic Rendering: Programming Touch Interaction with Virtual Objects." *Proceedings of the 1995 Symposium on Interactive 3D Graphics*. 1995. 123-130.

Seedhom, B B, E B Longton, V Wright, and D Dowson. "Dimensions of the Knee: Radiographic and Autopsy Study of Sizes Required for a Knee Prosthesis." *Ann Rheum Dis.*, 1972: 31:54-58.

Shoham, M, M Burman, E Zehavi, L Joskowicz, E Batkilin, and Y Kunicher. "Bone-Mounted Miniature Robot for Surgical Procedures: Concept and Clinical Applications." *IEEE Transactions on Robotics and Automation*, October 2003: 19(5):893-901.

Swanson, D K, and W J Book. "Path-Following Control for Dissipative Passive Haptic Displays." *Proceedings of the 11th Symposium on Haptic Interfaces for Virtual Environment and Teleoperator Systems*. 2003. 101-108.

Troccaz, J. United States of America Patent 5529159. 1996.

Troccaz, J, and Y Delnondedieu. "Semi-Active Guiding Systems in Surgery: A Two DOF-Prototype of the Passive Arm with Dynamic Constraints (PADyC)." *Mechatronics*, 1996: 6(4):399-421.

## **Appendix A – Assembly and Engineering Drawings**



## **Appendix B – Data Sheets for Major Components**

## **Appendix C – Budget**